# DUE GlobWave

## Deliverable D.16
## Satellite Wave Data Quality Report

| | | |
|---|---|---|
| Customer | : | ESA / ESRIN |
| Author | : | SatOC |
| ESRIN Contract Number | : | 21891/08/I-EC |
| Logica Project Reference | : | UK EC230943 |
| Document Reference | : | GlobWave/DD/SWDQR |
| Version/Rev | : | 1.2 |
| Date of Issue | : | 21 October 2010 |
| Category | : | A/I/P |

| | | |
|---|---|---|
| Prepared by<br>(SatOC, CLS) | Ellis Ash (SatOC), David Carter (SatOC), Fabrice Collard (CLS) | (Signature) |
| Reviewed by<br>(Logica) | Geoff Busswell<br>GlobWave Project Manager | (Signature) |
| Accepted by<br>(ESA/ESRIN) | Simon Pinnock<br>ESA Technical Officer | (Signature) |

# Amendment History

| Issue | Date | Status | Author |
|---|---|---|---|
| 0.1 | 30/07/10 | Complete draft for Altimetry parts | Ellis Ash |
| 0.2 | 23/08/10 | Complete draft of SAR parts | Fabrice Collard |
| 1.0 | 02/09/10 | Review and modifications | Geoff Busswell |
| 1.1 | 01/10/10 | Updates to address RIDS from ESA | Geoff Busswell |
| 1.2 | 21/10/10 | Updates on SAR Quality Criterion | Fabrice Collard |

# Distribution

| Name | Role | Company |
|---|---|---|
| Simon Pinnock | ESA Technical Officer | ESA |
| Geoff Busswell | GlobWave Project Manager | Logica |
| Harjit Sheera | GlobWave Deputy Project Manager | Logica |
| Jean-Francois Piolle | GlobWave Team, Ifremer Lead | Ifremer |
| Fabrice Collard | GlobWave Team, CLS Lead | CLS |
| Helen Snaith | GlobWave Team, NOCS Lead | NOCS |
| Dave Poulter | GlobWave Team, NOCS Scientist | NOCS |
| Ellis Ash | GlobWave Team, SatOC Lead | SatOC |
| GlobWave Community | | |

# Contents

# EXECUTIVE SUMMARY

This document is the Wave Data Quality Report for GlobWave.

There are three sets of analysis:

- A summary of the quality levels of the delayed-mode L2P data set.
- The L2P error characterisation using collocation measurements with *in situ* buoys.
- The L2P intercomparison using satellite crossover measurements.

The quality analysis shows different results for different sensors and generally the most modern instruments have the highest quality levels.

The error characterisation analysis provides an estimate of the significant wave height (Hs) standard error for individual measurements, and this will feed back into the Hs error variable of the L2P data set. For Altimetry, wave heights greater than 1m follow a linear function of Hs that varies with sensor. For wave heights less than 1m the errors are less certain and the error values for 1m will be used. For SAR, a crucial difference with previous studies is that the bias on Hss was found to be a function of dominant wavelength as well as the usual increase with swell height and decrease with wind speed.

The satellite crossover analysis generally shows good agreement between sensors. There are two exceptions to this that warrant further investigation: there is some nonlinearity between Topex and ERS1 at high significant wave heights, and the relationship between GFO and Jason-1 is anomalous for the year 2008, suggesting that GFO data from this year should be discarded.

# 1 INTRODUCTION

This document is the Satellite Wave Data Quality Report for GlobWave. It contains four main sections giving: 1) information on the quality of historical L2P data products, 2) results of the analysis of collocated altimeter and buoy data to derive estimates of the error on altimeter Hs, 3) results of the analysis of collocated SAR and buoy data to derive estimates of the error on SAR Hss 4) Results of the satellite crossover analysis. It represents deliverable D.16 of the DUE GlobWave Project.

We refer the reader to the Product User Guide and the GlobWave Portal for a full description of the GlobWave L2P data sets.

## 1.1 Document Structure

The document structure is as follows:

- Section 1 – Introduction: this section
- Section 2 – L2P Quality Analysis: Analysis of the quality levels of the delayed-mode L2P data set, presented by satellite and over the life of the satellite mission. Quality levels are averaged over the satellite cycle.
- Section 3 – Altimeter Hs Error Analysis: Analysis of the Altimeter buoy matchup data presented by satellite. Results give the standard deviations of matchups against Hs, comparison of L2P calibration and calibration derived from the analysis, and 95% limits of calibration that represent the Hs standard error.
- Section 4 – SAR Wave Spectra Error Analysis: Analysis of the SAR buoy matchup data presented by buoy network. Results give the calibration equations which are functions of the significant wave height, dominant direction and dominant wavelength.
- Section 5 – Satellite Crossover Analysis: Analysis of satellite crossover data for different Altimeter pairs.

## 1.2 Definitions and Acronyms

| Acronym | Definition |
|---|---|
| ASAR | Advanced Synthetic Aperture Radar |
| ASCII | American Standard Code for Information Interchange |
| CD | Compact Disc |
| CDIP | Coastal Data Information Program |
| CLS | Collecte Localisation Satellites |
| CNES | Centre National d'Etudes Spatiales |
| CSV | Comma Separated Value |
| DUE | Data User Element |

| Acronym | Definition |
|---|---|
| ENVISAT | ESA's Environmental Satellite |
| EO | Earth Observation |
| ERS | European Remote-Sensing Satellite |
| ESA | European Space Agency |
| ESRIN | ESA Space Research Institute |
| GDR | Geophysical Data Record |
| GEOSAT | GEOdetic SATellite |
| GFO | GEOSAT Follow On |
| Hs | Significant Wave Height |
| I/O | Input/Output |
| L2P | Level-2-Preprocessed |
| MDB | Match Up Database |
| NASA | National Aeronautical Space Administration |
| NDBC | National Data Buoy Center |
| NetCDF | Network Common Data Form |
| NOAA | National Oceanic and Atmospheric Administration |
| NOCS | National Oceanography Centre Southampton |
| NODC | National Oceanographic Data Center |
| NRT | Near Real Time |
| PDF | Portable Document Format |
| RMS | Root Mean Square |
| SAR | Synthetic Aperture Radar |
| SatOC | Satellite Oceanographic Consultants |
| SST | Sea Surface Temperature |
| TBC | To Be Confirmed |
| UKMO | United Kingdom Meteorological Office |

# 2 L2P QUALITY ANALYSIS

This section gives a summary of the quality levels of the GlobWave delayed-mode L2P wave data.

## 2.1 Quality criteria

Each Hs measurement in the L2P has an associated quality variable (swh_quality) that is assigned a quality level as follows:

| Value (decimal) | Meaning |
|---|---|
| 0 | Probably good measurement |
| 1 | Suspect, probably okay for some applications. For example this is set when rain is detected for an otherwise good measurement. |
| 2 | Probably bad measurement |
| 127 | Not evaluated |

The criteria used in evaluating these quality levels is described in Annex B of the L2P Product User Guide [D.5]. However, we note here that the quality evaluation criteria differs between each altimeter instrument according to the varying number and values of flags and instrument parameters included in the L2 source data. The results allow a broad comparison between the quality of retrieval of significant wave height from different altimeters, however direct comparison is more difficult and further work is required to understand the detailed differences between altimeter instruments.

## 2.2 Results

This section presents a summary of the quality levels of the L2P delayed-mode data. The quality levels for each L2P data file were counted and the values averaged over a repeat cycle of the satellite to take account of the variable influence of land within each file. Results give the percent of ocean data with good or suspect quality levels and are presented by satellite.

### 2.2.1 ERS1

For ERS-1 the repeat cycle was variable, either 3, 35 or 168 days.

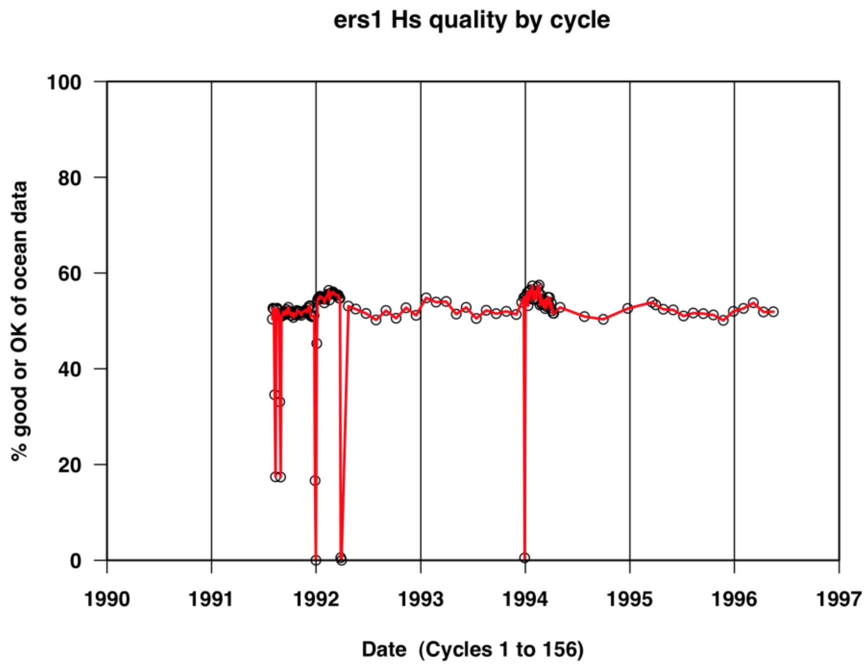


**Figure 2-1: Quality levels of L2P dataset for ERS1**

The results are given in Figure 2-1. Data quality levels are around 50% with some spikes indicating bad data in some cycles. The overall quality level can be attributed to noise of the altimeter instrument, causing about half of the data points to be rejected. There is a period at the start of the mission in 1991 with bad data quality as well as some cycles in 1992. One further cycle contains bad data quality at the start of 1994. These quality spikes are mostly from the 3-day repeat phase and are likely to represent short-term instrument issues or orbit manipulation phases.

### 2.2.2 ERS2

For ERS-2 the repeat cycle is constant at 35 days.

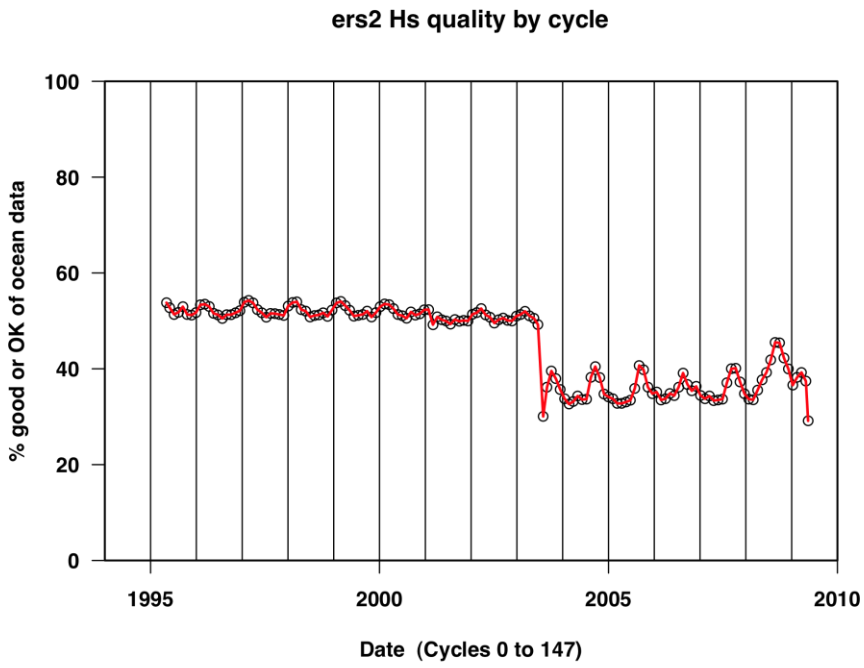


**Figure 2-2: Quality levels of L2P dataset for ERS2**

The results are given in Figure 2-2. Data quality levels are around 50% from 1995 to 2003 when there is a step reduction in quality to around 40% with an enhanced annual cycle. This corresponds to failure of the onboard recorder resulting in a loss of global data. From this point data were only received via direct download to ground stations and coverage was limited to the North Atlantic. More recently additional ground stations have been installed enabling increased coverage, including parts of the W Pacific, Indian and Southern oceans.

### 2.2.3 Envisat RA2

For Envisat the repeat cycle is the same as ERS-2 at 35 days.

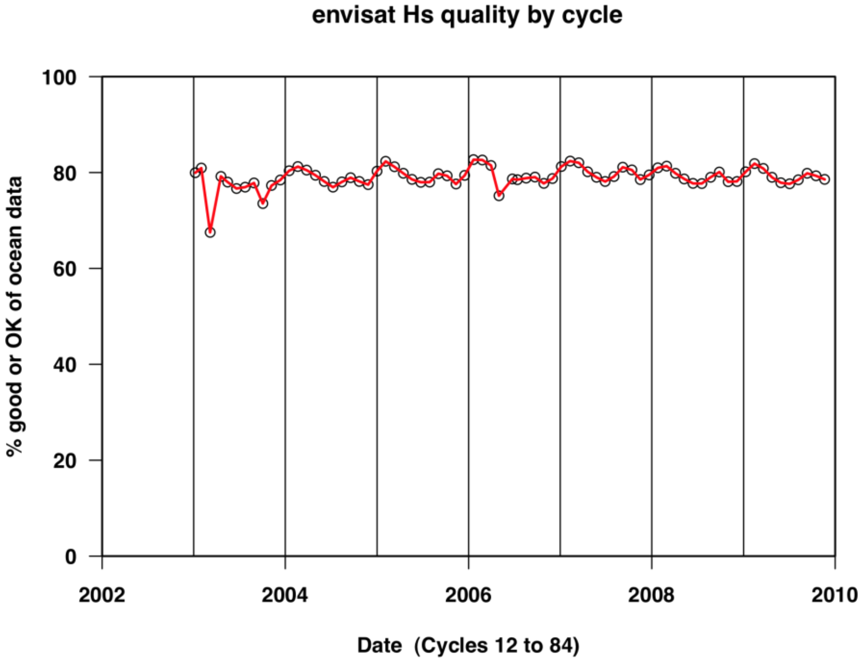


**Figure 2-3: Quality levels of L2P dataset for Envisat**

The results are given in Figure 2-3. The quality levels are higher than the ERS missions at around 80%. This is largely due to reduced noise level of the more modern altimeter instrument. There was a slightly lower quality level of two cycles in 2003 and one in 2006.

### 2.2.4 GEOSAT

For Geosat the repeat cycle was 17 days.

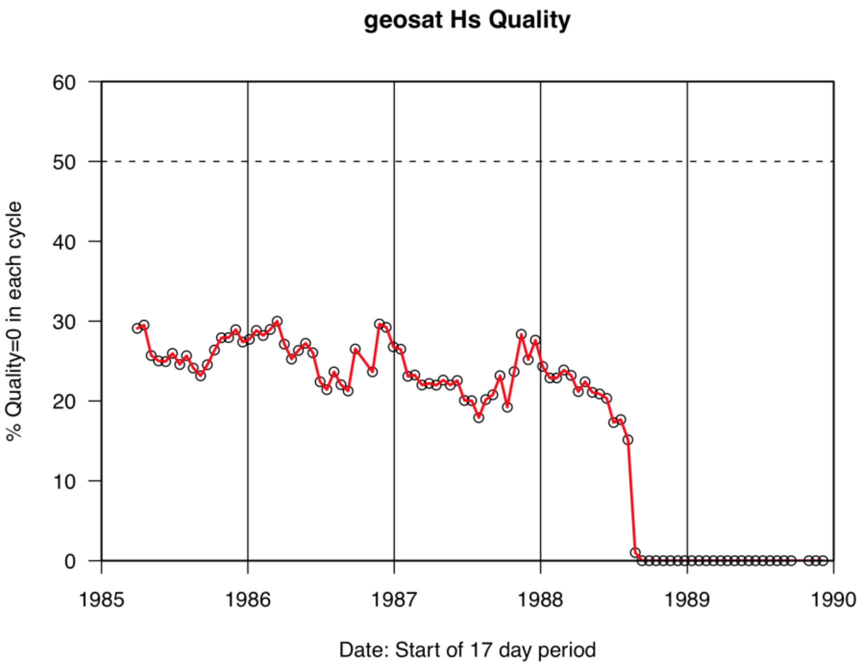


**Figure 2-4: Quality levels of L2P dataset for GEOSAT**

The results are given in Figure 2-4. Geosat was the first successful altimeter mission with global coverage and provides the only useful data of the 1980s. The quality levels are lower than subsequent missions at below 30%. In August 1988 the satellite suffered from attitude control problems and there were no good quality measurements after that time.

### 2.2.5 GEOSAT Follow-On

For GEOSAT Follow-On (GFO) the repeat cycle was 17 days.

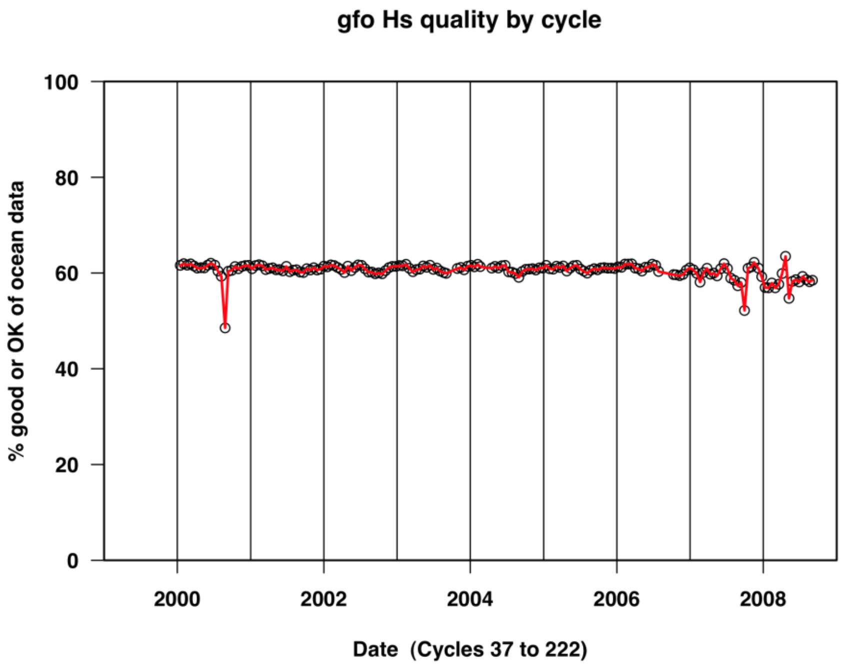


**Figure 2-5: Quality levels of L2P dataset for GFO**

The results are given in Figure 2-5. Data quality levels are consistent at around 60%. One cycle in 2000 has reduced quality levels, and the quality towards the end of the mission was more variable.

### 2.2.6 TOPEX/Poseidon

For TOPEX/Poseidon the repeat cycle is 10 days.

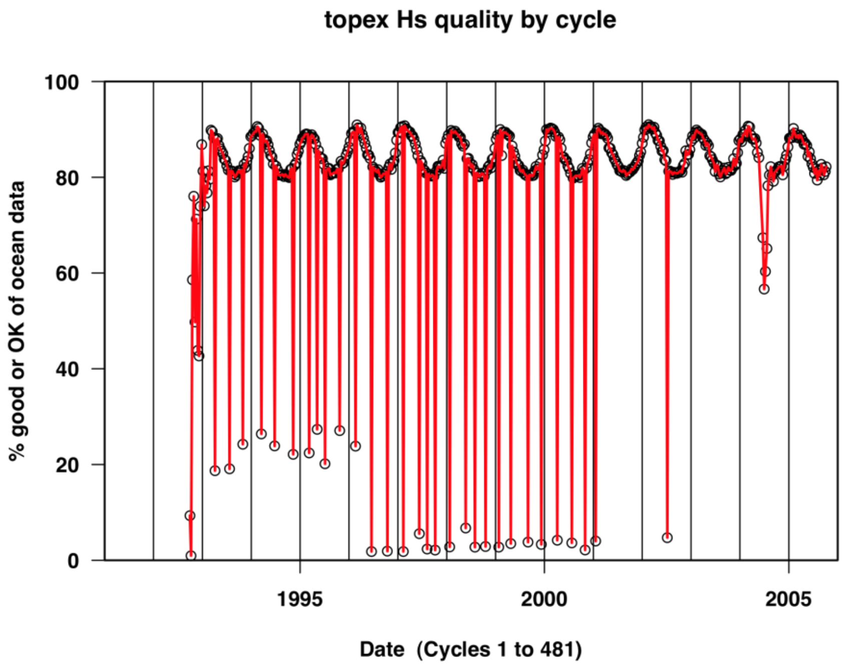


**Figure 2-6: Quality levels of L2P dataset for TOPEX/Poseidon**

The results are given in Figure 2-6. There are obvious spikes of cycles with poor quality data and these correspond to the Poseidon sensor that operated about 5% of the time. The spikes are a feature of the quality analysis rather than the data themselves as the Poseidon instrument was known to work well. The quality problems are likely to result from the checks on a particular flag in the L2 source data which seems to be set over-cautiously for Poseidon. The reliability of this flag is known to be problematic, especially in the first two-thirds of the mission. The criteria used for the quality analysis for Poseidon data will be refined in order to try and remove these quality spikes in a future update of the L2P dataset.

For TOPEX data the quality levels are between 80 and 90%, and there is a pronounced annual cycle due to the greater influence of Antarctic ice compared to Arctic ice at the inclination of the TOPEX/Poseidon mission (66 degrees).

### 2.2.7 Jason-1

The Jason-1 mission follows TOPEX/Poseidon and the repeat cycle is the same at 10 days.

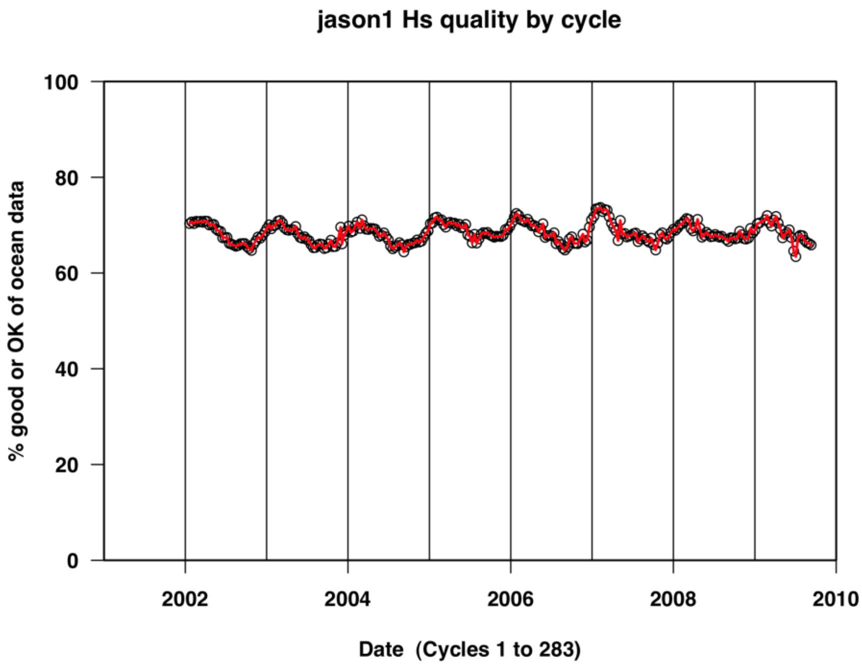


**Figure 2-7: Quality levels of L2P dataset for Jason-1**

The results are given in Figure 2-7. Quality levels are around 70% and there is some variability within the annual cycle. The reduced quality compared to TOPEX is likely to be a feature of the quality criteria, though it is worth noting that Jason-1 uses the Poseidon-type altimeter which is a more modern instrument.

### 2.2.8 Jason-2

For Jason-2 the repeat cycle is 10 days.

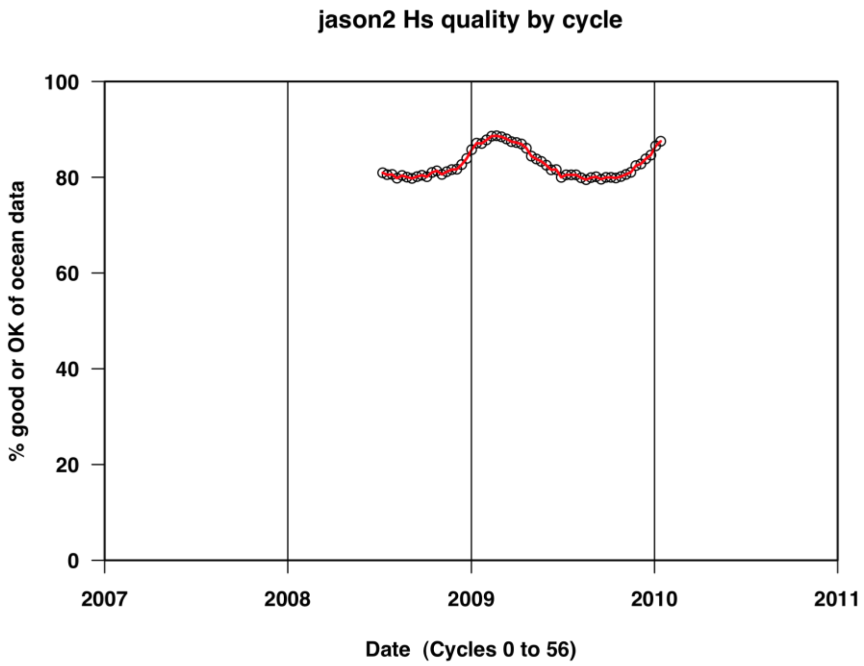


**Figure 2-8: Quality levels of L2P dataset for Jason-2**

The results are given in Figure 2-8. Quality levels are between 80 to 90% with a pronounced annual cycle due to the greater influence of Antarctic ice at the inclination of the Jason missions.

### 2.2.9 Envisat ASAR

Envisat ASAR Level2 wave spectra quality is assessed primarily by its capability to provide reliable information on significant wave height, dominant wavelength and dominant direction. Figure 2-9 illustrates the percentage of data where SAR imagettes are of good quality for wave inversion, allowing the significant wave height to be retrieved with a value above the RMS error of 30cm. It can be seen that after mid 2004 the percentage stabilises around 90%.

Whereas significant wave height and dominant wavelength can usually be retrieved, unambiguous dominant propagation direction can only be retrieved if the imaginary part of the cross spectra is above the noise floor. If this constraint is satisfied then wave motion can be detected by comparing two looks of the ocean surface separated by 0.32 sec. Figure 2-10 illustrates the percentage of directionally unambiguous retrieved spectra and shows a reasonably stable figure of about 62%. The remaining 38% are composed of 32 ambiguously retrieved spectra and 6 bad quality wave spectra, mostly caused by non wave signatures on the SAR images among which 2% are due to partial land coverage within the image.

With the extra post-processing done for the L2P GlobWave products, we have now the possibility to provide the propagation direction ambiguity independently for each partition of the retrieved wave spectrum, and not only for the whole spectrum. The percentage of directionally unambiguous retrieved partitions of the wave spectra has been calculated (Figure 2-11 and Figure 2-12). From mid 2004 onward, we observe an average of 72% for the most energetic partition in each spectra and an average of 51% for the second most energetic partition in each spectra. It appears that, on average, the most energetic wave partition has lower propagation direction ambiguity. For each specific spectrum, the user now has the ability to select only the partitions of the wave spectra for which the ambiguity is removed which was not possible from the original L2 products.

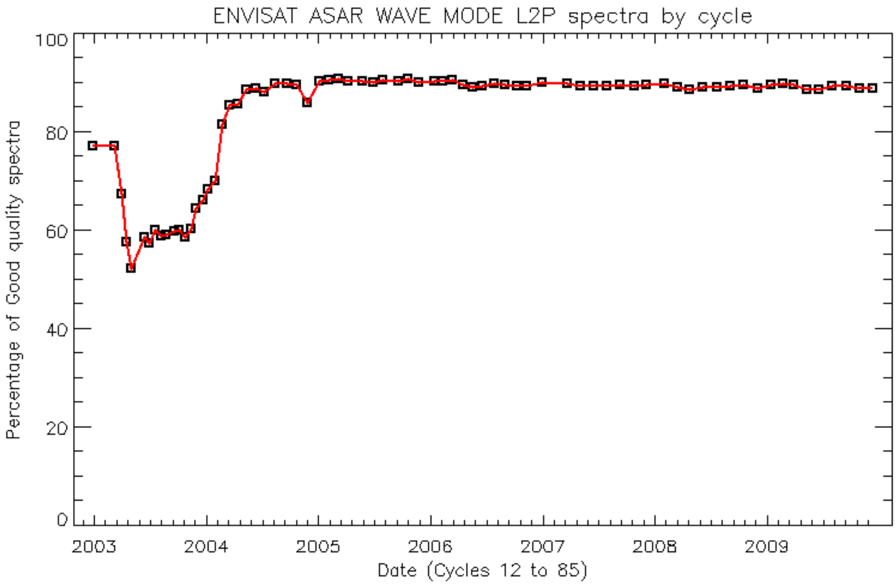


**Figure 2-9: Quality levels of L2P SAR spectra dataset for ENVISAT**

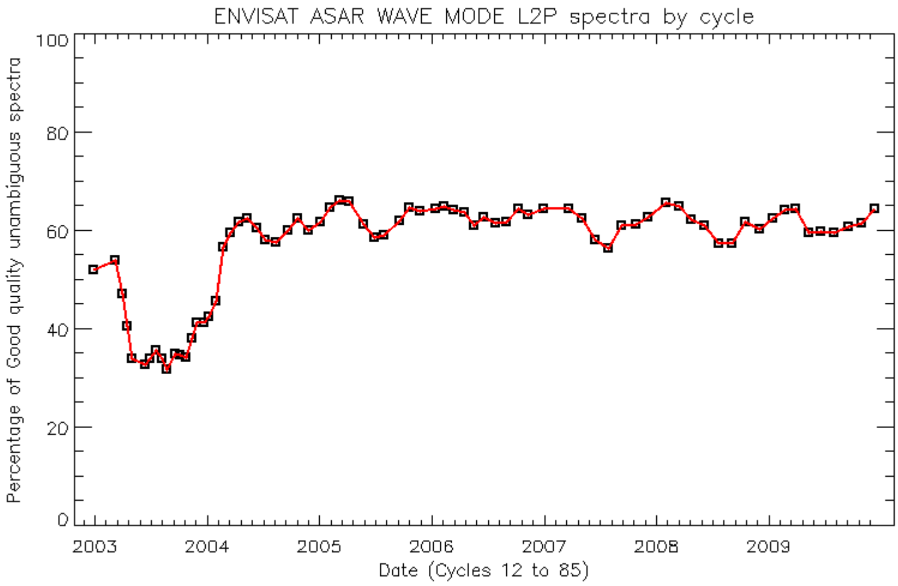


**Figure 2-10: Quality levels of L2P SAR unambiguous spectra dataset for ENVISAT**

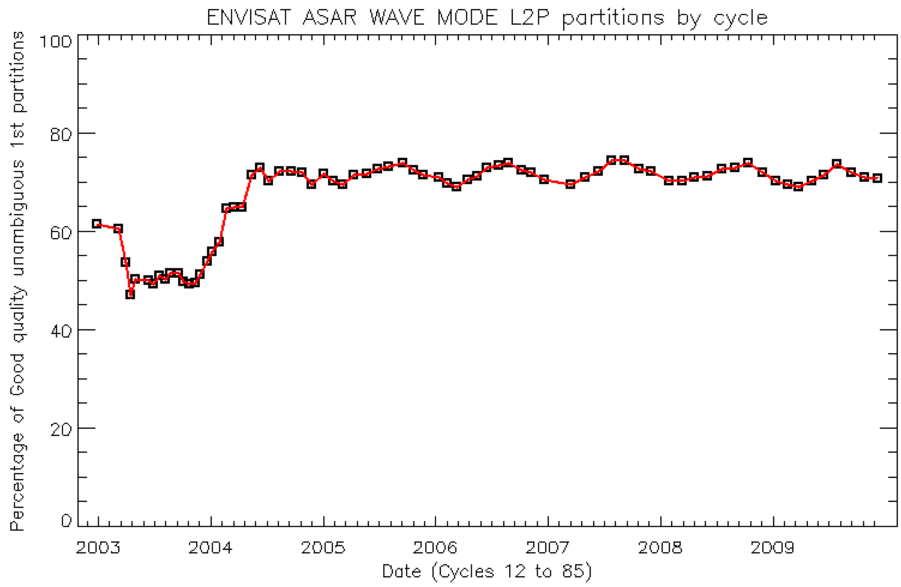


**Figure 2-11: Quality levels of L2P SAR most energetic partitions for ENVISAT**

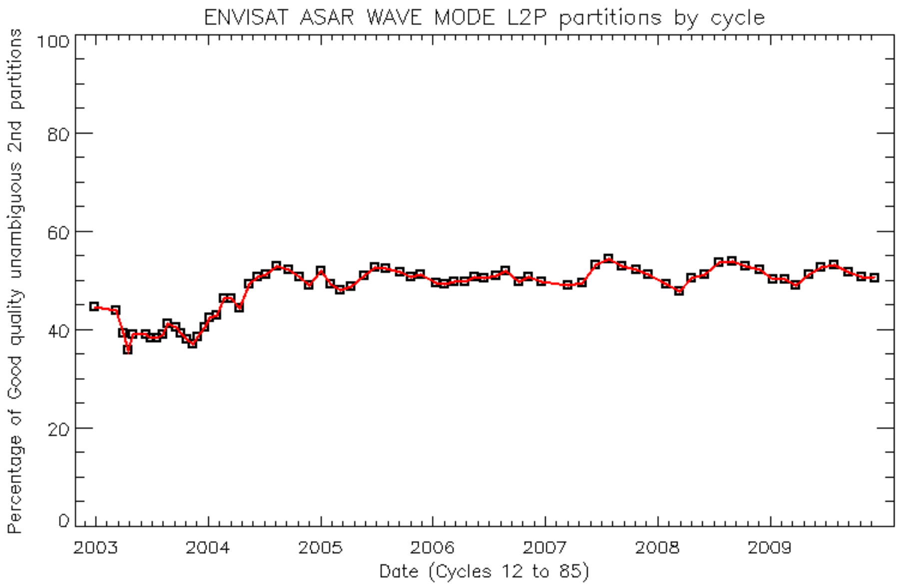


**Figure 2-12: Quality levels of L2P SAR second most energetic partitions**

## 2.3 Miscellaneous quality issues

This section presents miscellaneous quality issues with the L2 source data that were identified during the processing stage. These problems are inherited by the L2P data files.

### 2.3.1 Envisat RA2

There were quality issues with 2 Envisat RA2 GDR files:

- Cycle 039, orbit 002: there are 2709 measurements specified in the header and only 2689 available

- Cycle 047 orbit 194: there are some bad latitude values (808) and corrupt times

### 2.3.2 GEOSAT Follow-On

533 GFO L2 source data files from different cycles (about 38 days in total) were found to contain no data, and these passes are omitted from the L2P data set.

# 3 ALTIMETER HS ERROR ANALYSIS

The Hs error analysis has been carried out with the altimetry wave data using a quality-controlled dataset of collocations with *in situ* buoys.

## 3.1 Matchup data

Altimeter-buoy and SAR-buoy matchup data were produced using the GlobWave *in situ* database. This contains quality-controlled networks from the following buoy networks:

- NODC – US Buoy network in Atlantic and Pacific
- CDIP – Mainly coastal buoys around N America and Pacific Islands
- UKMet – UK Met Office buoys around UK
- OPPE – Spanish buoys in Atlantic and Mediterranean
- POSEIDON – Greek buoys in the Mediterranean

The matchup criteria for a satellite pass is 100km in distance and 1 hour in time. Matchups are available for all L2P data sets except GEOSAT, and are made available via ftp in the same way as the L2P data.

To derive the Hs standard error for altimetry only matchup data from offshore buoys, those more than 300km from the coast, were used. This is because nearer to the coast wave heights often vary significantly over very small distances, so the matchup criteria have a greater contribution to the variability and would need to be tuned accordingly. Also the altimeter performance near the coast is more variable and depends on the direction of the pass. There are problems when any land is in the altimeter footprint, and the sensor takes time to readjust to ocean conditions when flying off the land. This results in a larger proportion of data failing quality checks limiting the data available for analysis.

In practice only NODC buoy matchups were used as these contain the majority of offshore buoys. There are also known differences between measurements from different buoy networks (Cotton, 1998; Durrant and Greenslade, 2007) and selecting a single network removes the effect of these differences.

In order to compare the different buoy networks the error analysis for Envisat was also performed for CDIP, UKMet and OPPE networks (the POSEIDON data not being ready in time). The results are shown in section 3.3.3 below.

## 3.2 Analysis method

This section describes the method used to obtain prediction limits on individual altimeter (1 Hz) estimates of significant wave height (*Hs*) from comparisons of altimeter and buoy data.

From data sets of altimeter and open ocean buoy *Hs* obtained within 100 km and 1 hour of each other, the first step is to calibrate the altimeter *Hs* by estimating the parameters $\alpha$ and $\beta$ in

$$Hs_{buoy} = \alpha + \beta \, Hs_{alt} \tag{1}$$

This is done by Orthogonal Distance Regression (ODR), using the package ODRPACK – see Bloggs et al. (1989) – making the following assumptions:

A.1 There are no systematic errors in the buoy data

A.2 Calibration is obtained from a linear relationship between the altimeter and the buoy data

A.3 The sampling variability of the altimeter and buoy data are equal

A.4 The sampling variability is constant, independent of the magnitude of *Hs*.

Assumption A.4 is not strictly justified. The variability of both altimeter and buoy *Hs* increases with *Hs*; so the ODR gives undue emphasis to the high *Hs*, but these are relatively few in number.

The estimate of *Hs*, $\hat{Hs}$, is then, from Assumption 1:

$$\hat{Hs} = \alpha + \beta \, Hs_{alt} \tag{2}$$

So, having obtained $\hat{Hs}$, an estimate of *Hs*, we need to derive its standard error, i.e. we want the variance of $Hs - \hat{Hs}$. We have from Assumption 3 that:

$$Var(Hs - Hs_{buoy}) = Var(Hs - Hs_{alt}) \tag{3}$$

Since

$$Var(Hs_{alt} - Hs_{buoy}) = Var([Hs - Hs_{buoy}] - [Hs - Hs_{alt}]) \tag{4}$$

with the further assumption:

A.5 The sampling errors on the buoy *Hs* and the altimeter *Hs* are independent

then

$$Var([Hs - Hs_{buoy}] - [Hs - Hs_{alt}]) = Var(Hs - Hs_{buoy}) + Var(Hs - Hs_{alt}) = 2\,Var(Hs - Hs_{alt}) \tag{5}$$

Now,

$$Var(Hs - \hat{Hs}) = Var(Hs - \alpha - \beta \, Hs_{alt}) = Var(Hs - \beta \, Hs_{alt})$$

but $\beta \approx 1$ so

$$Var(Hs - \hat{Hs}) \approx Var(Hs - Hs_{alt}) \tag{6}$$

Indeed, it is a moot point whether Assumption 3 refers to the calibrated or uncalibrated values of $Hs_{alt}$.

Therefore, from Eq.s 3 to 6:

$$Var(Hs - \hat{Hs}) \approx {}^{1}/_{2}\, Var(Hs_{buoy} - Hs_{alt}) \qquad (7)$$

The estimated 95% range of $\hat{Hs}$ is given by $\approx \hat{Hs} \pm q\, {}^{1}/_{\sqrt{2}}\, sd(Hs_{buoy} - Hs_{alt})$ where $q$ is the 0.025 and 0.975 quantiles of the Student-t distribution with $NN - 2$ d.o.f. ($NN$ is the number of pairs of buoy and altimeter data.)

In practice, to get around the problem that Assumption 3 is not justified, Equation 7 is applied ”piecewise” to values of $Hs_{alt}$ in 0.5 m steps from 1 m up. (Errors on $Hs$ < 1 m are relatively large; the altimeter is less accurate here, and altimeter and buoy data are rounded.) The estimated $sd(Hs_{buoy} - Hs_{alt})$ from each step are regressed against $Hs_{alt}$ to obtain a linear relationship; the values are weighted by $1/\sqrt{NN}$ .

In the plots of $sd(Hs - \hat{Hs})$ below the red lines are approximate 95%ile ranges of the estimated sd’s.

The regression line gives $sd$ as a linear function of $Hs_{alt}$ and the 95% range on $\hat{Hs}$ is then $\approx \hat{Hs} \pm q\, sd$. The value of $q\, sd$ is included in the L2P data as the measure of error.

We could widen this 95% range to take into account the uncertainties in $\alpha$ and $\beta$ in Eq. 2, but in practice (large $NN$) these uncertainties are minuscule compared to that calculated from $sd$.

## 3.3 Results

The results are presented by satellite for ERS-1, ERS-2, Envisat, GFO, TOPEX/Poseidon, Jason-1 and Jason-2 respectively (for Geosat no buoy matchups are available). For most altimeters there are three plots as follows:

- Position of buoys from which matchup data were used
- Results of standard deviation with 95% confidence ranges and linear fit, calculated over 0.5m intervals for Hs > 1m.
- Results of ODR analysis with 95% limits and comparison with calibration used in initial release of the L2P data.

For Envisat there are additional sets of plots for the different buoy networks: NODC, UKMet, OPPE, CDIP and POSEIDON. A comparison of the standard error values is given in

Table **3-1**. The analysis of the few UKMet buoys gives errors that for the majority of Hs values lie within the NODC analysis, so there is no evidence from this network to increase the standard error values.

With the OPPE, CDIP and POSEIDON networks the analysis included buoys much closer to the coast. Errors are correspondingly higher and this can be attributed to coastal factors, in particular the greater variability of the wave field such that the matchup criteria has a much larger influence on the analysis. In fact for the POSEIDON buoys, because of the small statistical sample and very large spread we felt that it was not possible to perform a meaningful error analysis. Therefore for the reasons outlined the matchup measurements for the CDIP, OPPE and POSEIDON buoys cannot be considered to represent the same wave field for many of these data points, hence the analysis with these coastal networks is included for interest but not used in the calculation of standard error values.

For TOPEX/Poseidon the analysis was broken down into three time periods due to the switch from radar transmitter A to transmitter B and the period of measurement drift in the preceding years. The errors during the drift phase (from 1996 to 1998) were found to lie within the limits for the A transmitter from 1992 to 1995, so these A transmitter error values will also be used for the drift period.

In general the error analysis was not broken down into smaller time periods, such as annually, as this would result in a small sample size. Instead the variation of altimeter performance with time is covered in the crossover analysis presented in section 5.

A summary of the Hs error values resulting from the analysis is given in Table 3-2 contained within section 3.4.

### 3.3.1 ERS-1

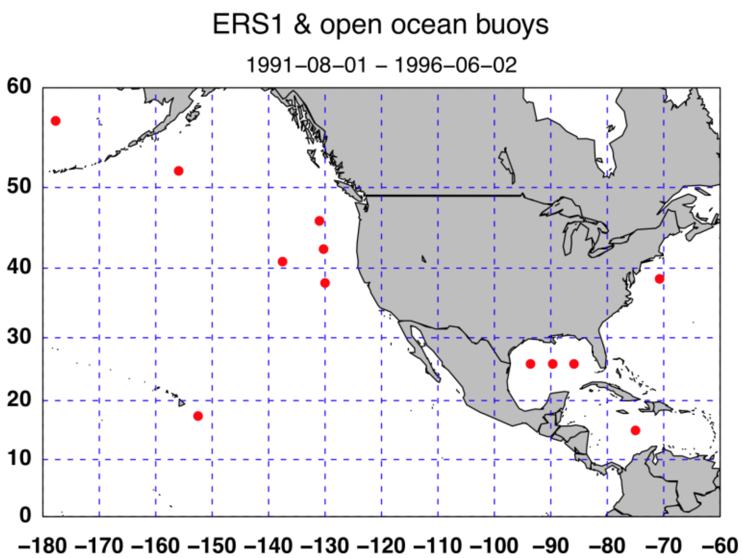


**Figure 3-1: Buoys used for ERS-1 error analysis**

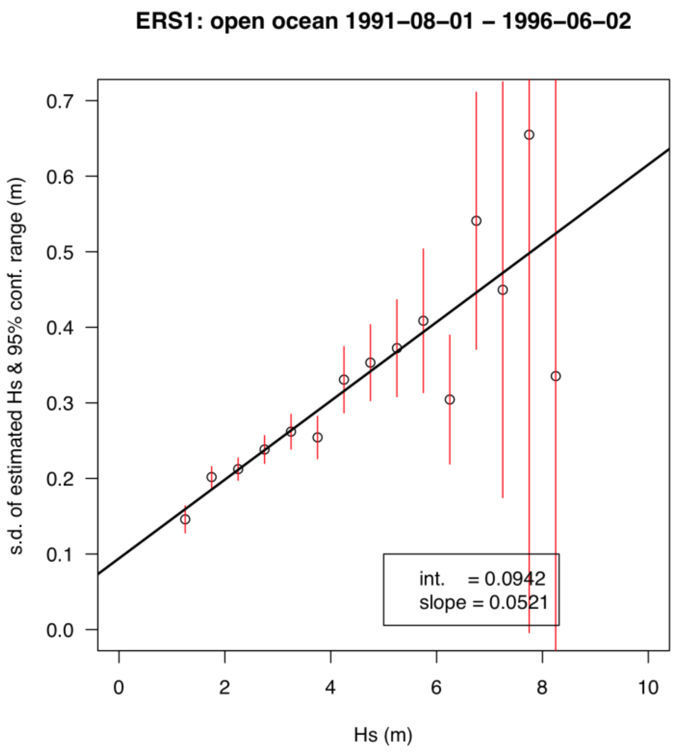


**Figure 3-2: Standard deviations of Hs and 95% confidence ranges for ERS-1**

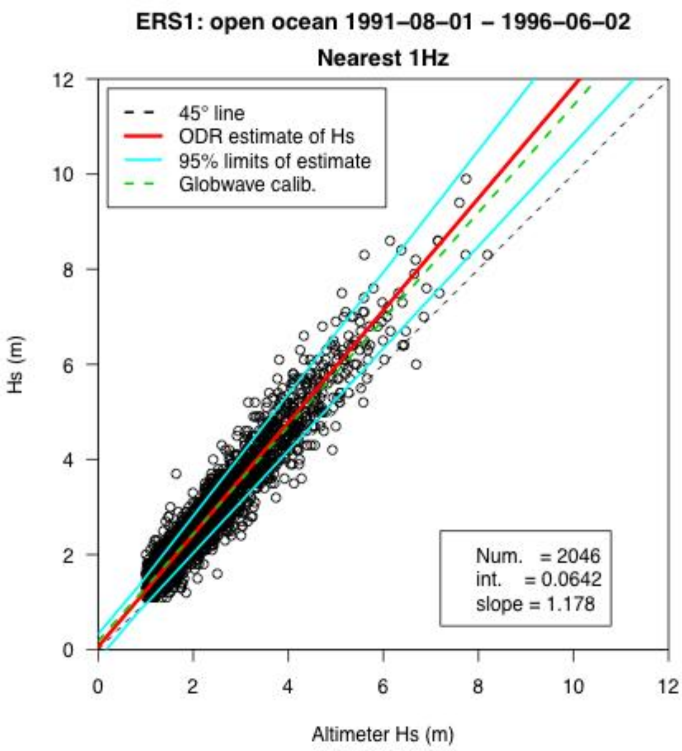


**Figure 3-3: Calibration comparison and 95% error limits for ERS-1**

### 3.3.2 ERS-2

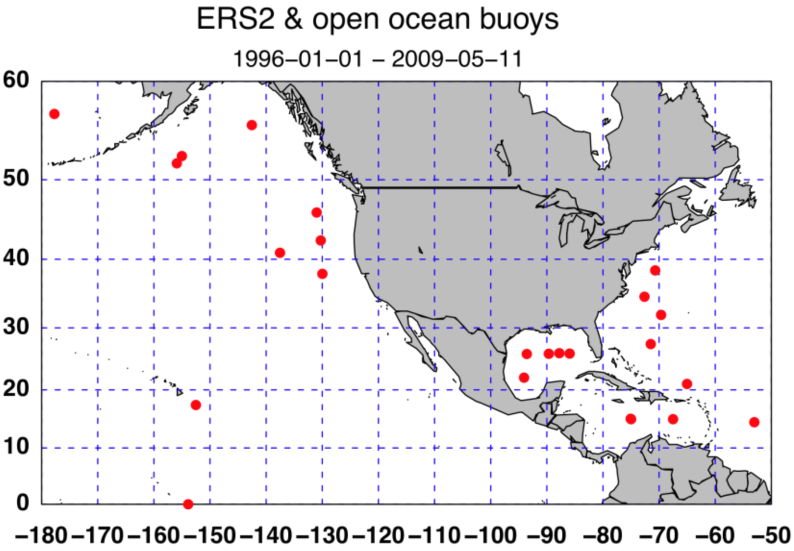


**Figure 3-4: Buoys used for ERS-2 error analysis**

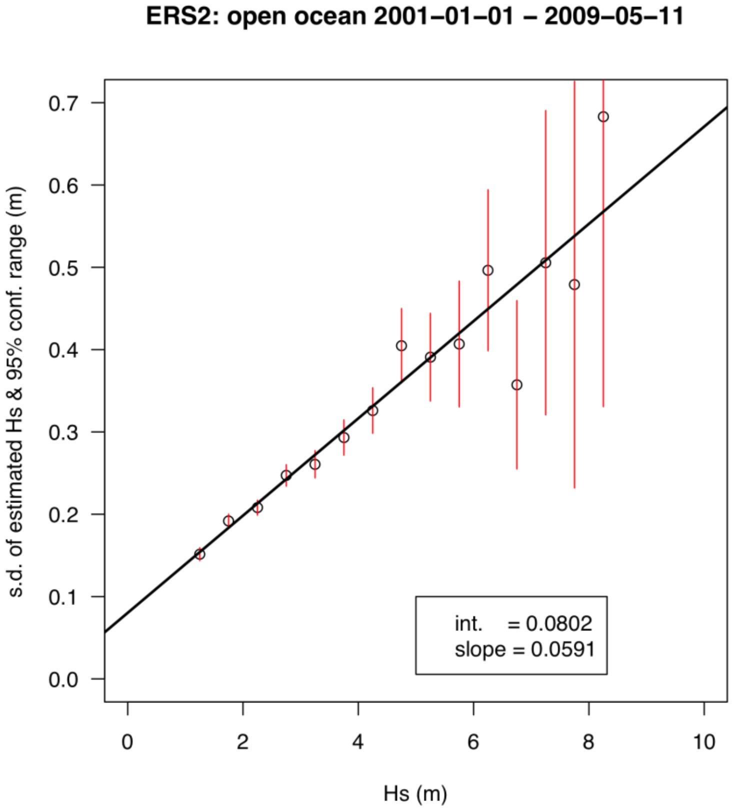


**Figure 3-5: Standard deviations of Hs and 95% confidence ranges for ERS-2**

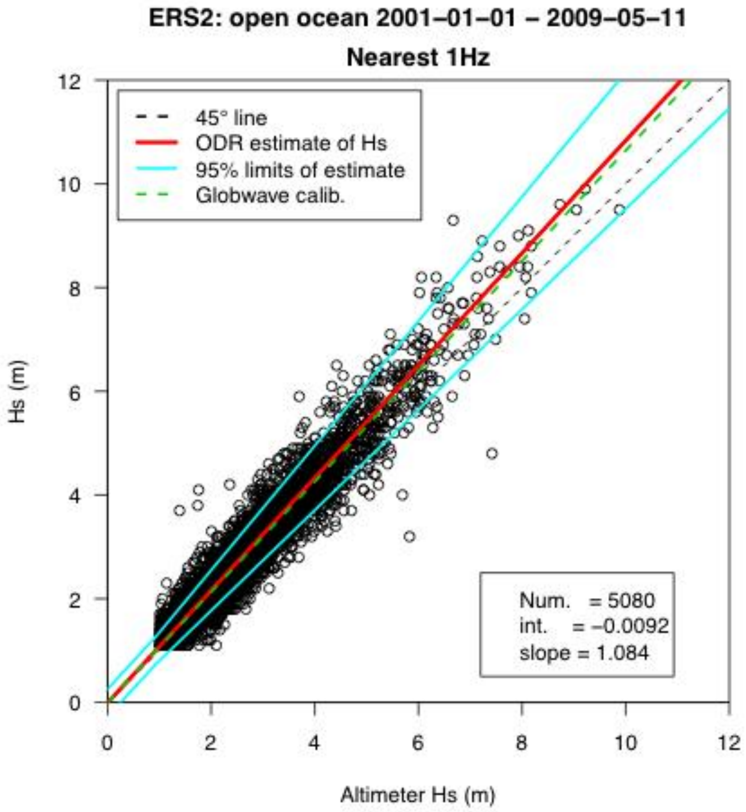


**Figure 3-6: Calibration comparison and 95% error limits for ERS-2**

### 3.3.3 Envisat

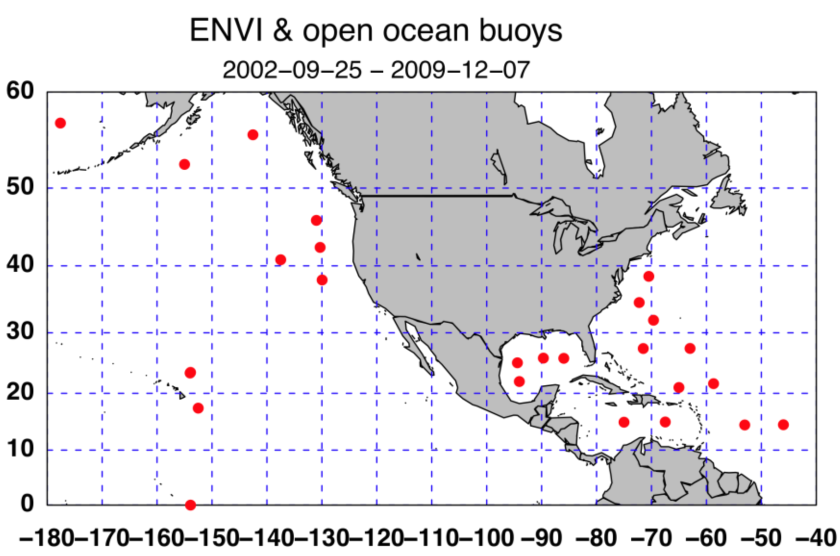


**Figure 3-7: Buoys used for Envisat error analysis**

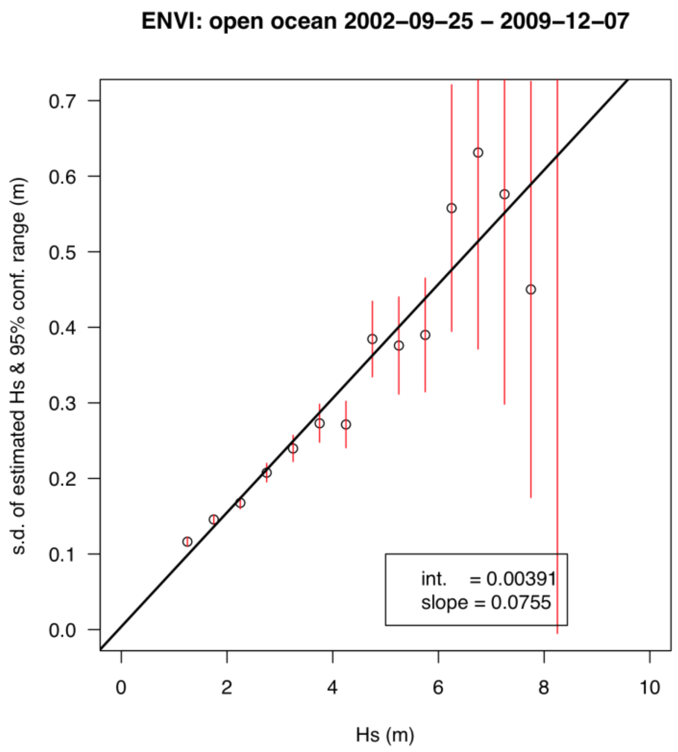


**Figure 3-8: Standard deviations of Hs and 95% confidence ranges for Envisat**

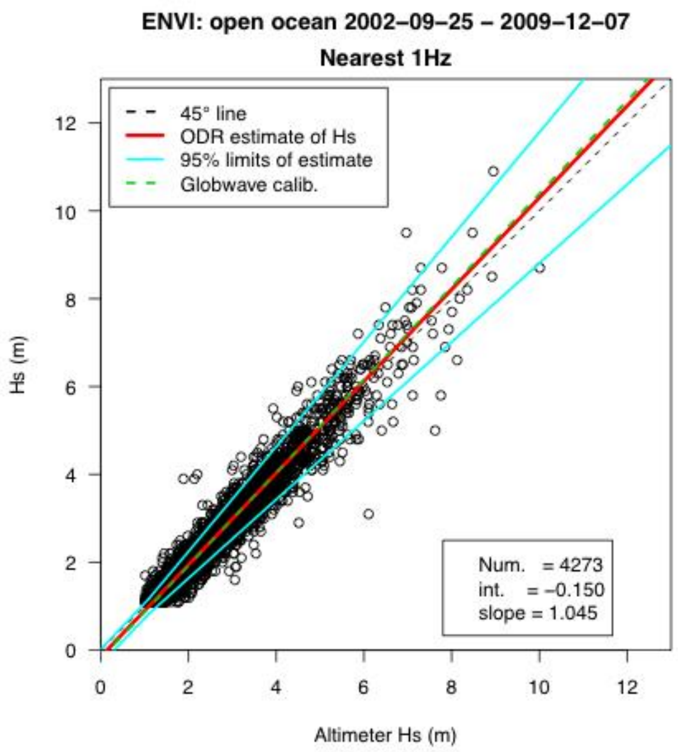


**Figure 3-9: Calibration comparison and 95% error limits for Envisat**

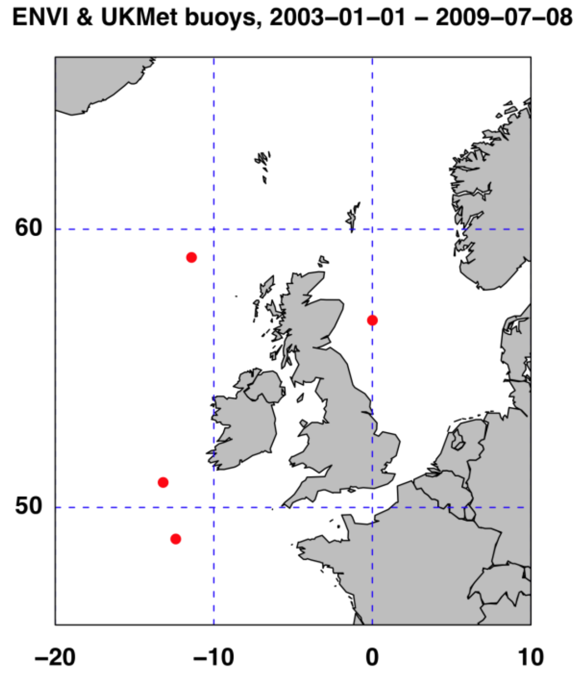


**Figure 3-10: Buoys used for Envisat error analysis with UKMet network**

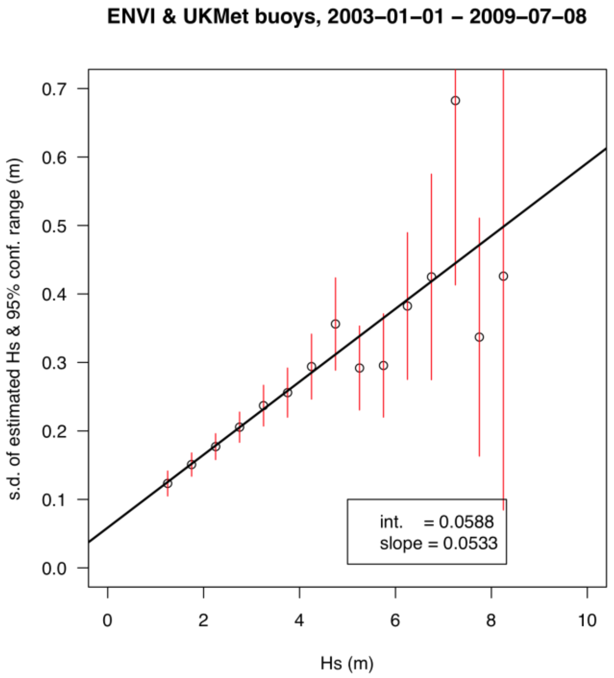


**Figure 3-11: Standard deviations of Hs and 95% confidence ranges for Envisat with UKMet buoys**

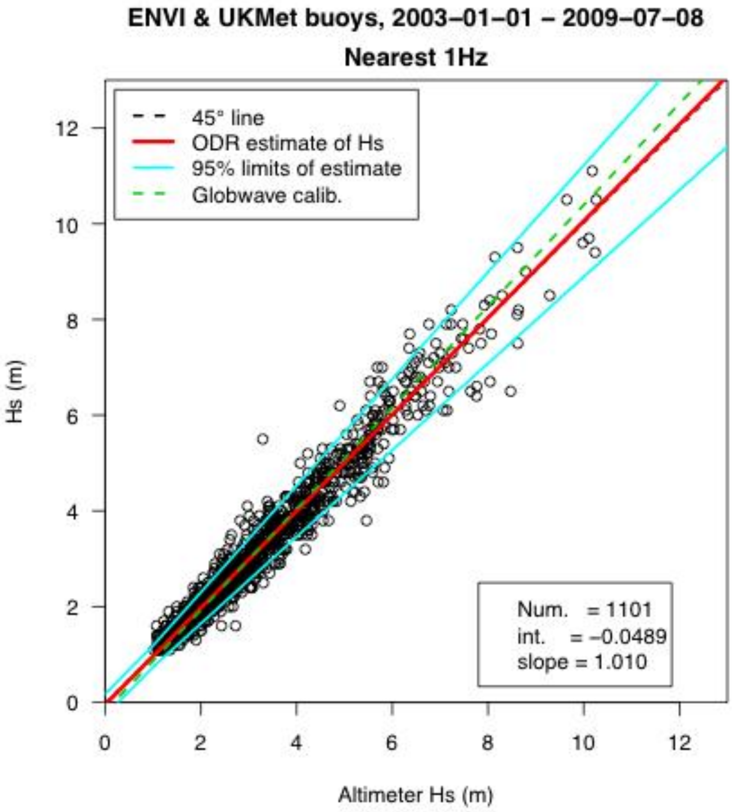


**Figure 3-12: Calibration comparison and 95% error limits for Envisat with UKMet buoys**

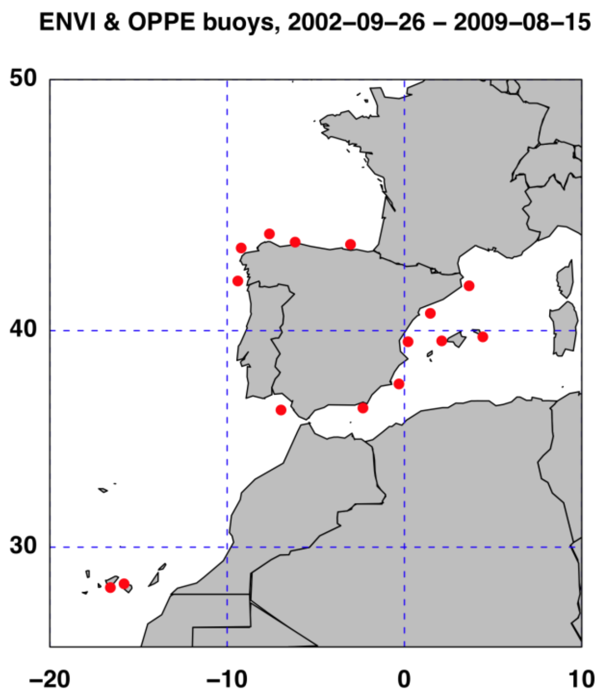


**Figure 3-13: Buoys used for Envisat error analysis with OPPE network**

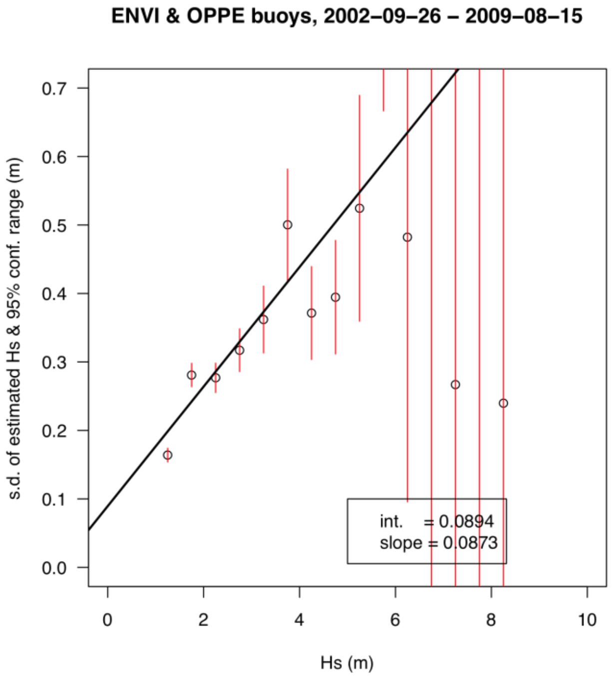


**Figure 3-14: Standard deviations of Hs and 95% confidence ranges for Envisat with OPPE buoys**

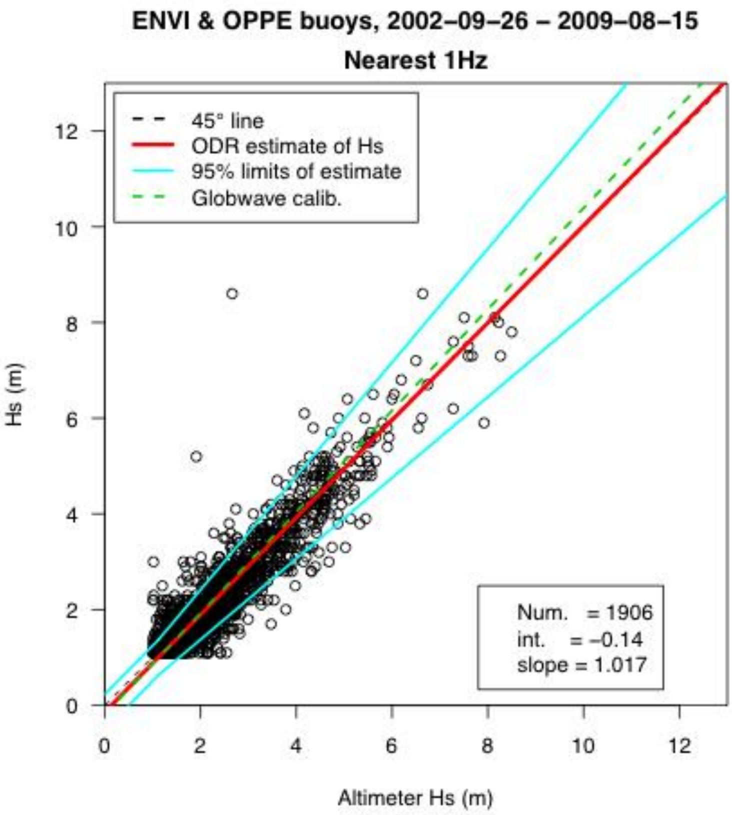


**Figure 3-15: Calibration comparison and 95% error limits for Envisat with OPPE buoys**

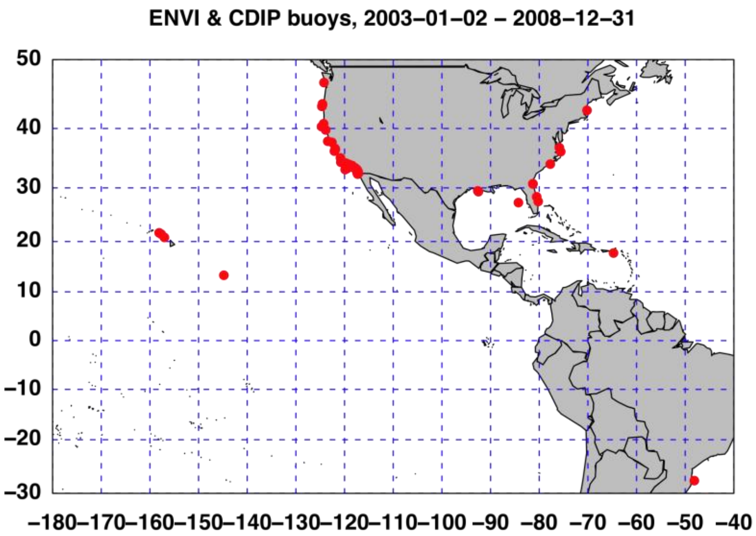


**Figure 3-16: Buoys used for Envisat error analysis with CDIP network**

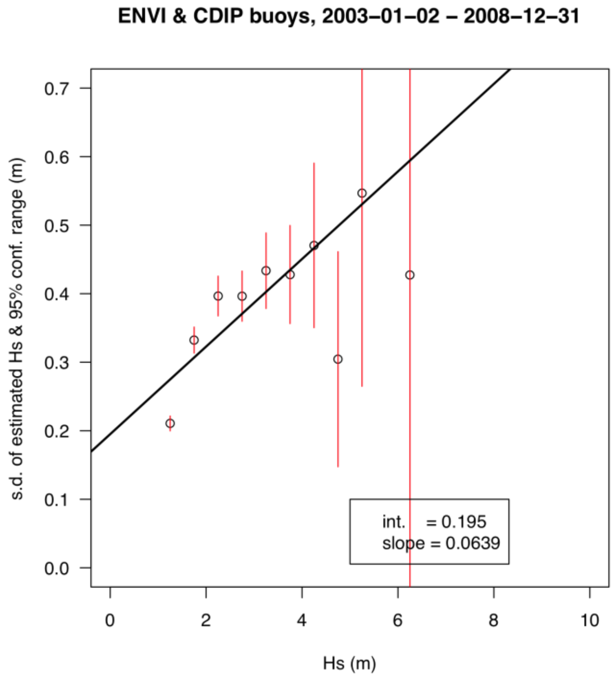


**Figure 3-17: Standard deviations of Hs and 95% confidence ranges for Envisat with CDIP buoys**

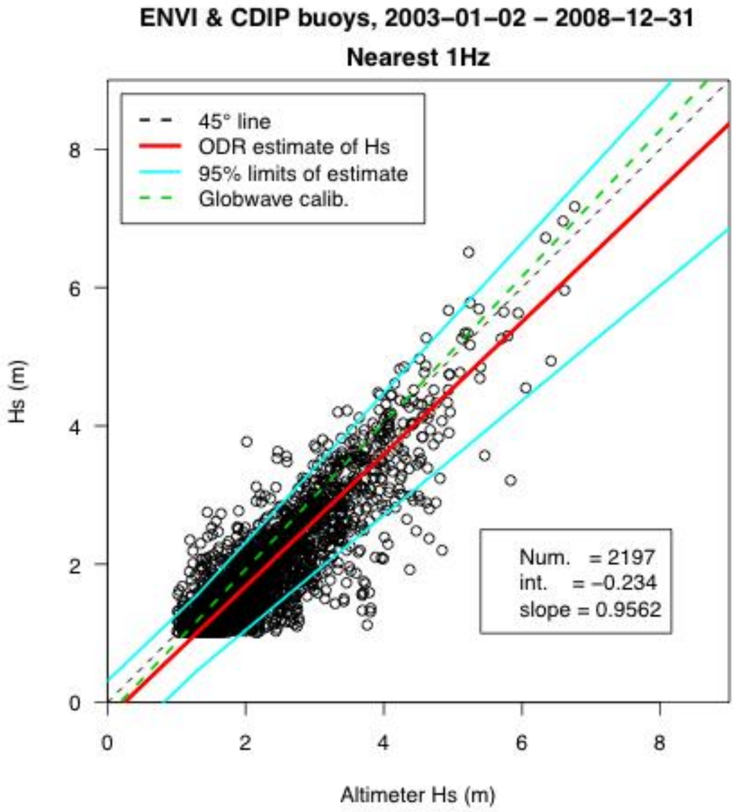


**Figure 3-18: Calibration comparison and 95% error limits for Envisat with CDIP buoys**

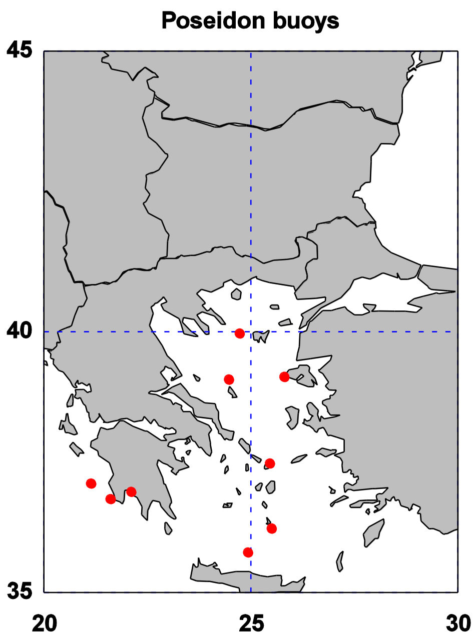


**Figure 3-19: Buoys used for Envisat error analysis with POSEIDON network**

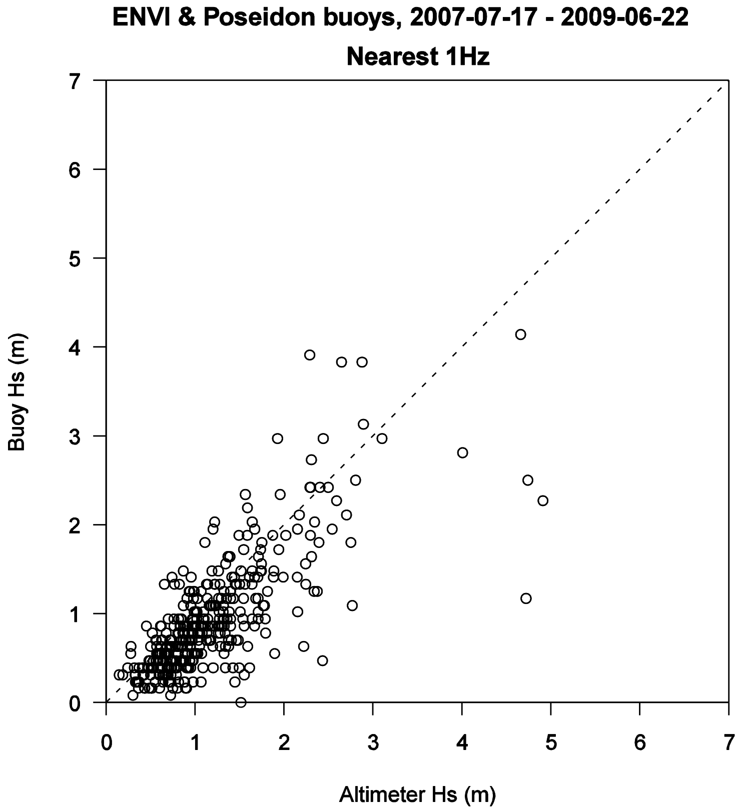


**Figure 3-20: Calibration comparison and 95% error limits for Envisat with CDIP buoys**

Unfortunately for the Envisat/POSEIDON analysis only 115 matchup pairs with Hs>1 were found. Because of the small statistical sample and large spread we felt that it was not possible to perform a meaningful error analysis. The map in Figure 3-19 gives the buoy locations and these illustrate the close proximity to the coast of many of the buoys, which is not conducive to a comparison with an Altimeter. Also, using the current Altimeter-buoy collocation distance could in principle mean that the observations were taken on different sides of one of the islands, further explaining the large spread.

A comparison of the error estimates for the different buoy networks is given below.

| Buoy Network | Formula (Hs > 1m) | SE (Hs <= 1m) | SE (Hs = 4m) | SE (Hs = 8m) |
|---|---|---|---|---|
| NODC | 0.004 + Hs*0.076 | 0.080 | 0.308 | 0.612 |
| UKMet | 0.059 + Hs*0.054 | 0.113 | 0.273 | 0.487 |
| OPPE | 0.089 + Hs*0.087 | 0.176 | 0.438 | 0.787 |
| CDIP | 0.195 + Hs*0.064 | 0.259 | 0.451 | 0.706 |
| POSEIDON | N/A | N/A | N/A | N/A |

**Table 3-1: Comparison of the Envisat error estimates for the different buoy networks**

### 3.3.4 Geosat

No matchup data are available for Geosat as the mission predates the buoy networks.

### 3.3.5 Geosat Follow-On

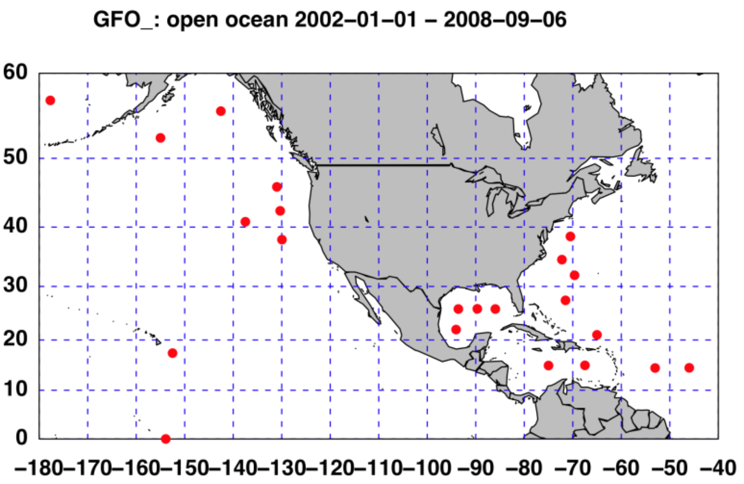


**Figure 3-21: Buoys used for GFO error analysis**

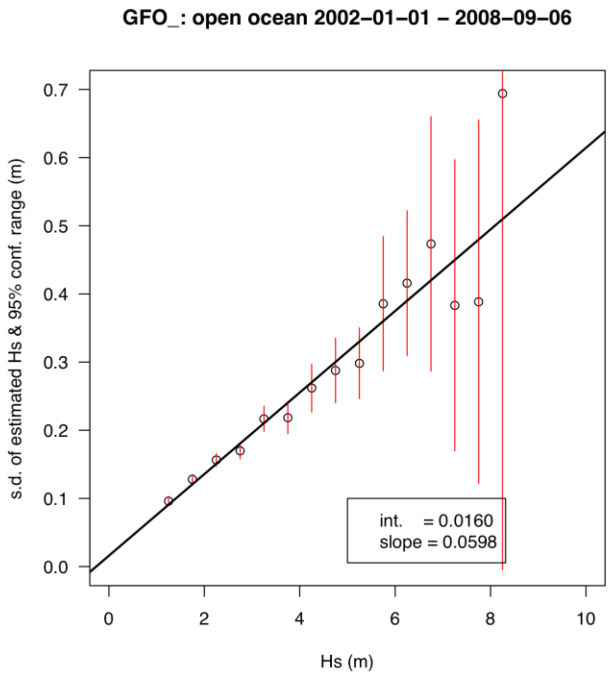


**Figure 3-22: Standard deviations of Hs and 95% confidence ranges for GFO**

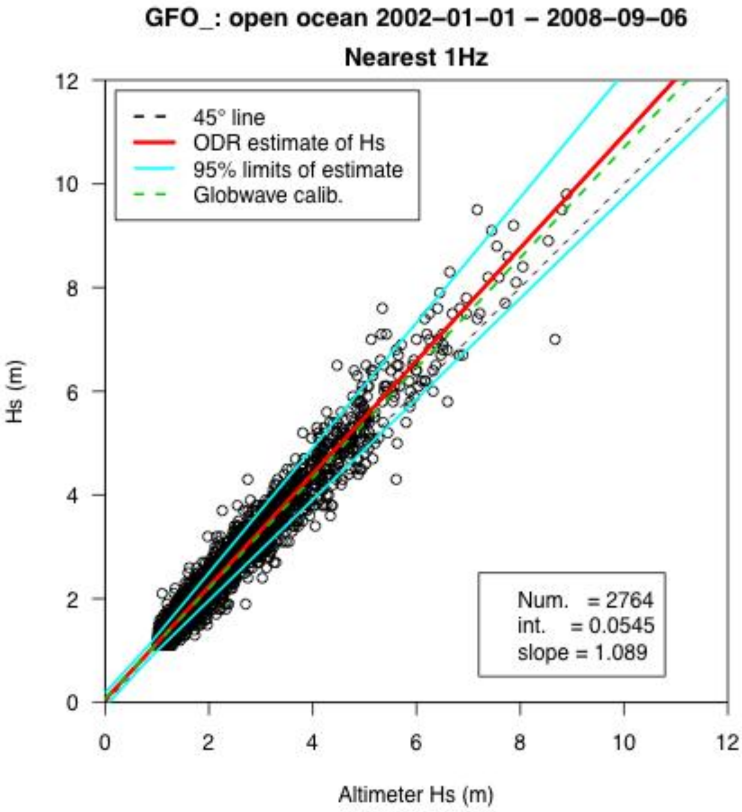


**Figure 3-23: Calibration comparison and 95% error limits for GFO**

### 3.3.6 TOPEX/Poseidon

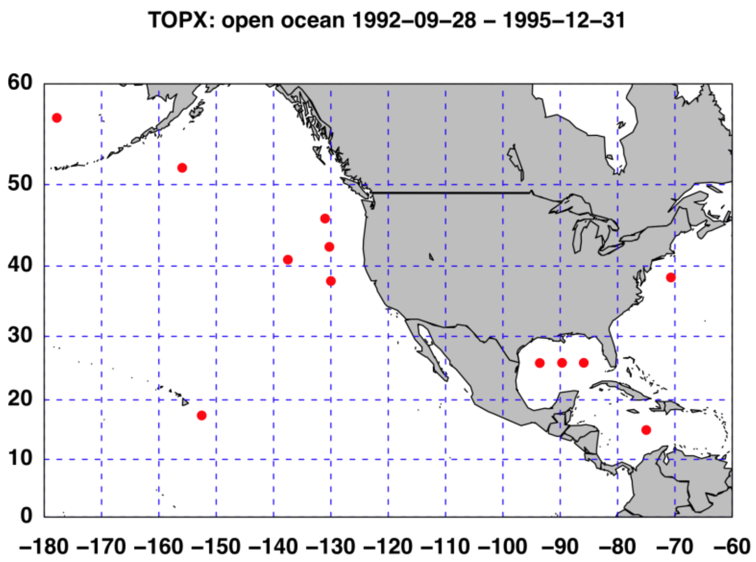


**Figure 3-24: Buoys used for TOPEX A error analysis**

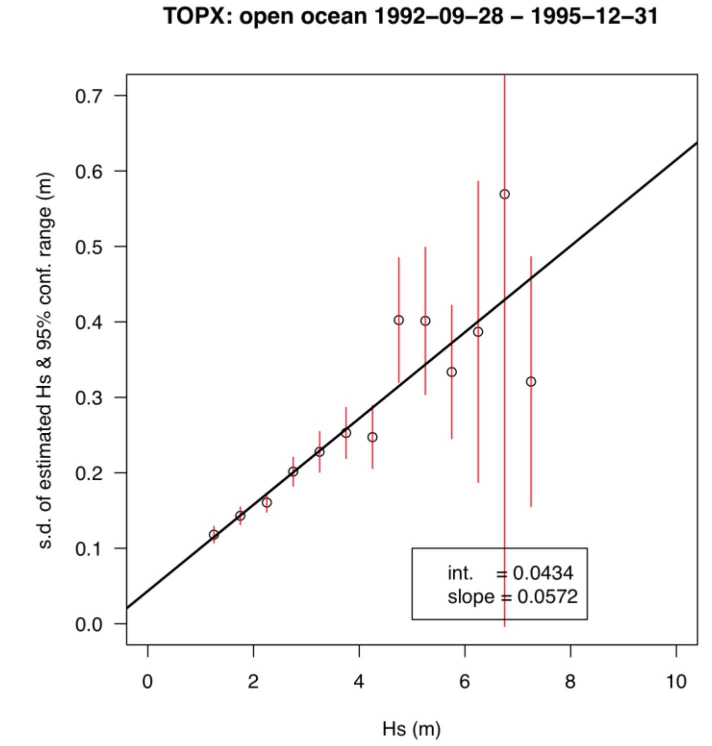


**Figure 3-25: Standard deviations of Hs and 95% confidence ranges for TOPEX A**

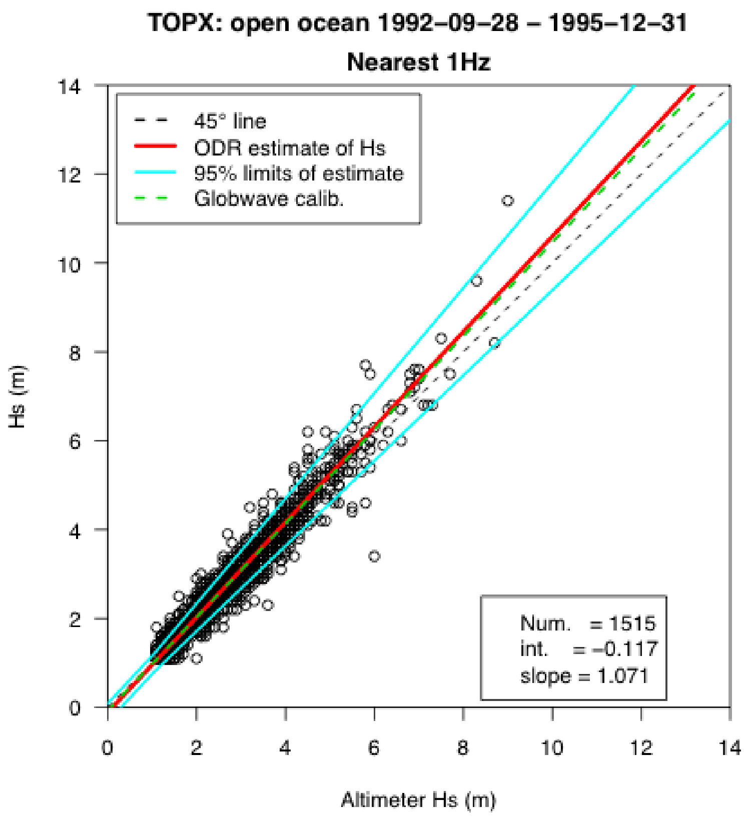


**Figure 3-26: Calibration comparison and 95% error limits for TOPEX A**

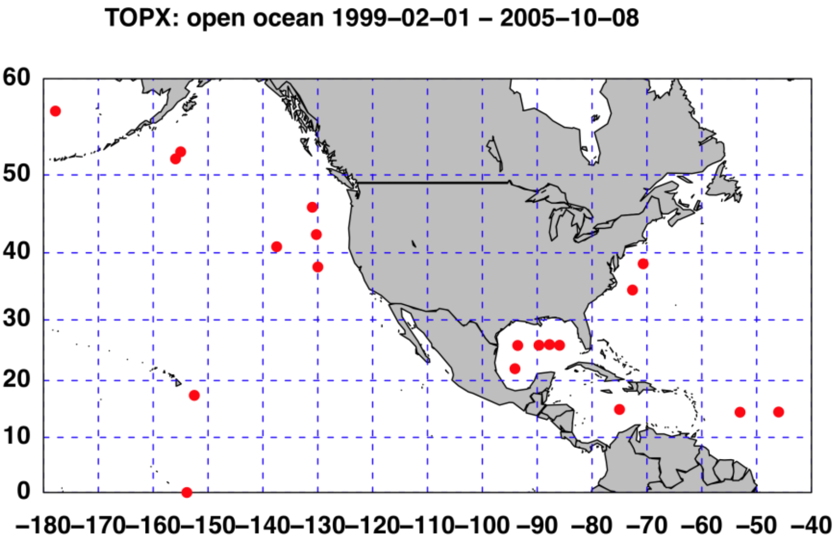


Figure 3-27: Buoys used for TOPEX B error analysis

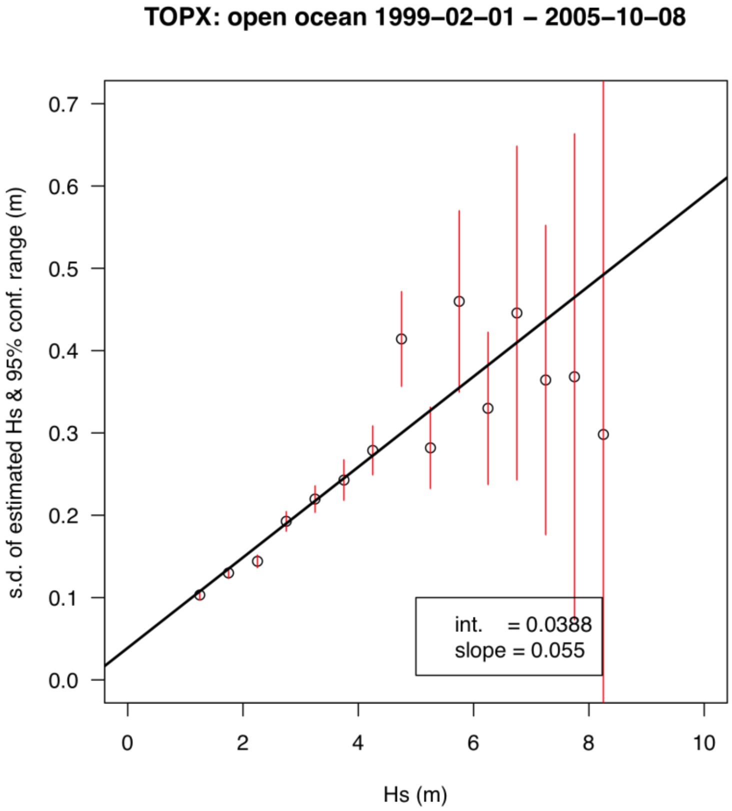


Figure 3-28: Standard deviations of Hs and 95% confidence ranges for TOPEX B

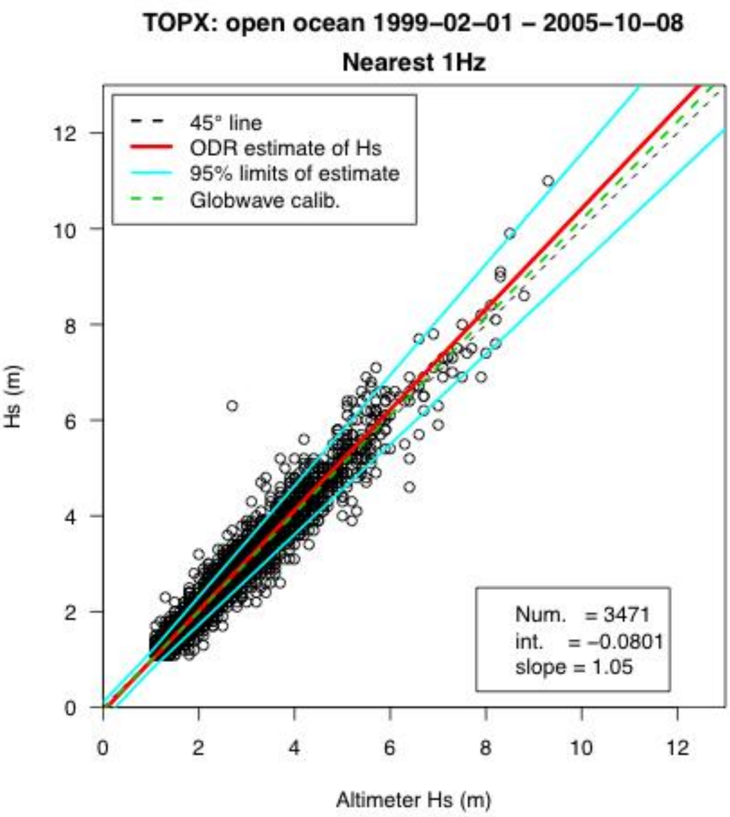


**Figure 3-29: Calibration comparison and 95% error limits for TOPEX B**

### 3.3.7 Jason-1

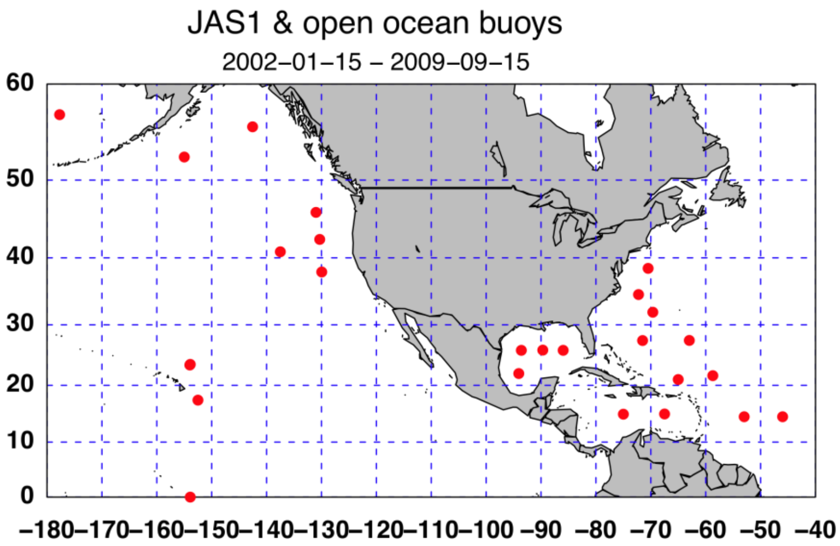


**Figure 3-30: Buoys used for Jason-1 error analysis**

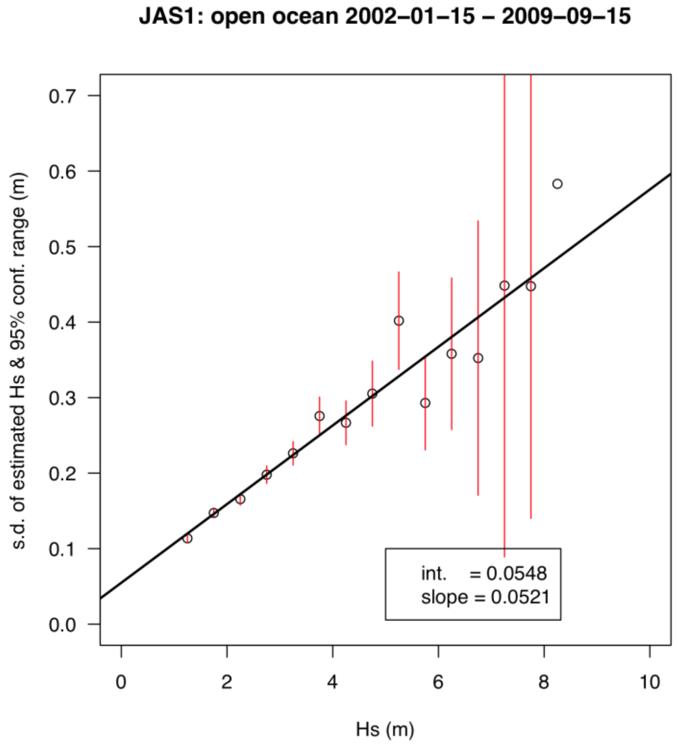


**Figure 3-31: Standard deviations of Hs and 95% confidence ranges for Jason-1**

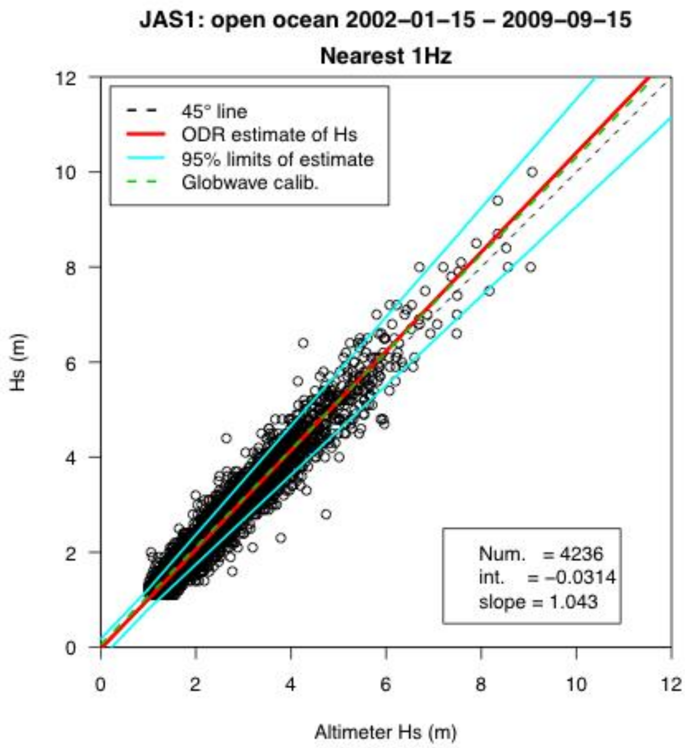


**Figure 3-32: Calibration comparison and 95% error limits for Jason-1**

### 3.3.8 Jason-2

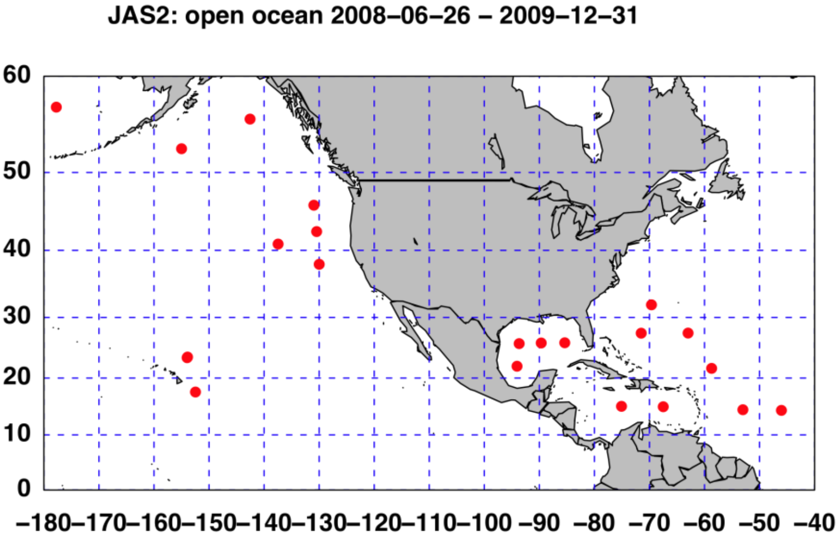


**Figure 3-33: Buoys used for Jason-1 error analysis**

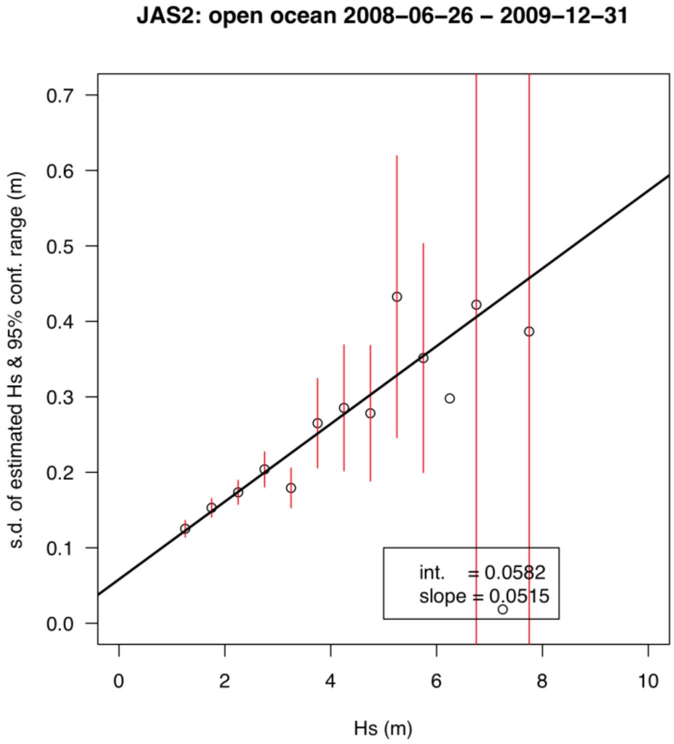


**Figure 3-34: Standard deviations of Hs and 95% confidence ranges for Jason-1**

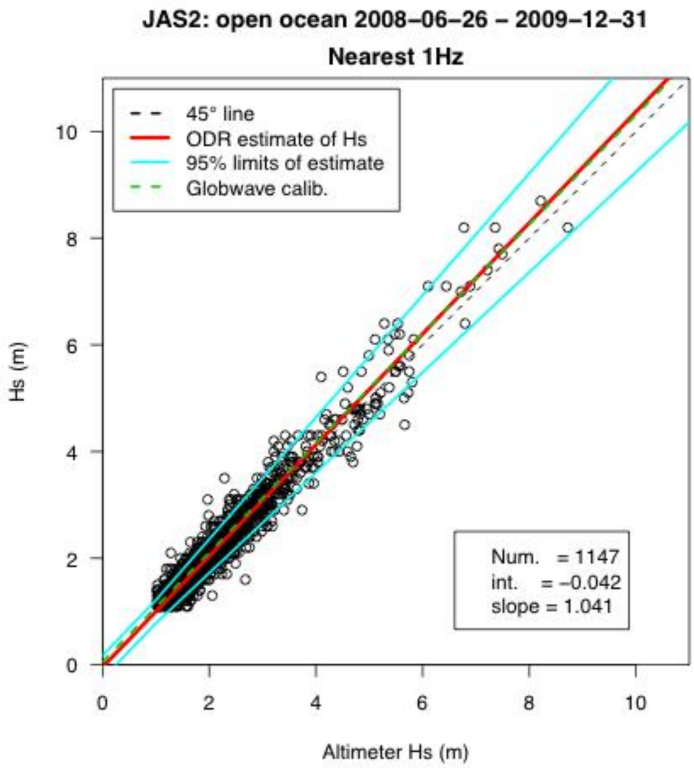


**Figure 3-35: Calibration comparison and 95% error limits for Jason-1**

## 3.4 Error Estimates

The following table gives the algorithms for calculating standard error bands for inclusion in the altimetry L2P data, with error ranges given by the calibrated Hs ± these values. The range corresponds to about half the vertical distance between the light blue lines in the ODR results figures above, as 95% confidence limits equals 1.96 x standard error.

| Altimeter | Formula (Hs > 1m) | SE (Hs <= 1m) | SE (Hs = 4m) | SE (Hs = 8m) |
|---|---|---|---|---|
| ERS-1 | 0.094 + Hs*0.052 | 0.146 | 0.303 | 0.511 |
| ERS-2 | 0.080 + Hs*0.059 | 0.139 | 0.317 | 0.554 |
| Envisat | 0.004 + Hs*0.076 | 0.080 | 0.306 | 0.608 |
| GFO | 0.022 + Hs*0.058 | 0.080 | 0.253 | 0.484 |
| TOPEX A | 0.043 + Hs*0.057 | 0.101 | 0.272 | 0.501 |
| TOPEX B | 0.039 + Hs*0.055 | 0.094 | 0.259 | 0.480 |
| Jason-1 | 0.055 + Hs*0.052 | 0.107 | 0.263 | 0.471 |
| Jason-2 | 0.058 + Hs*0.052 | 0.110 | 0.264 | 0.470 |

**Table 3-2: Algorithms for Calculating Standard Error Bands for Inclusion in the Altimetry L2P Data**

## 3.5 References

Bloggs, P. T., Byrd, R. H., Rogers, J. E., and Schnabel, R. B. 1989.
Odrpack - software for weighted orthogonal distance regression.
ACM Transactions on Mathematical Software, 15(4):348–364.

P. D. Cotton 1998.
A feasibility study for a global satellite buoy intercalibration experiment.
SOC Research & Consultancy Report No. 26, 73pp. (Unpublished manuscript prepared for the BNSC ENVISAT Exploitation Programme)

Durrant, T. H. and Greenslade, D. J. M. 2007.
Validation and application of Jason-1 and Envisat significant wave heights.
In Proc 10th Int. Workshop on wave hindcasting and forecasting, Oahu, Hawaii, USA, November 2007.

# 4 SAR WAVE SPECTRA ERROR ANALYSIS

The SAR wave spectra error analysis has been carried out with the SAR L2P wave data using a quality-controlled dataset of collocations with *in situ* buoys.

## 4.1 Matchup data

SAR-buoy matchup data were produced using the GlobWave *in situ* database. This contains quality-controlled networks from the following buoy networks:

- NODC – US Buoy network in Atlantic and Pacific
- CDIP – Mainly coastal buoys around N America and Pacific Islands
- UKMet – UK Met Office buoys around UK
- OPPE – Spanish buoys in Atlantic and Mediterranean
- POSEIDON – Greek buoys in the Mediterranean

However only NODC and CDIP network provide directional wave spectral moments that can be used to construct an estimate of 2D (frequency and direction) wave spectra to be partitioned and compared with SAR 2D (wavenumber and direction) wave spectra.

The usual matchup criteria for a satellite pass is 100km in distance and 1 hour in time. Taking advantage of the dynamical information available from SAR L2P datasets, we have developed a co-location methodology that goes further than just selecting data within a given spatial and temporal distance.

For each swell system detected during SAR wave spectra partitioning, we make use of the dominant wavelength and dominant direction to determine the surface wave group velocity vector and determine the time at which the observed wave train will eventually arrive in the vicinity of a given buoy location. This principle allows us to obtain a "dynamical" co-location between an observation and a buoy that are further apart than the typical distance used. This means that a larger larger matchup database can be used, providing more statistically robust estimates. However, this methodology assumes no modification of swell system properties along propagation from observation to buoy location. Surface wave theory supports this assumption in terms of wavelength and direction (propagation along great circles) in deep water, but wave energy or significant wave height do vary along the propagation. We have verified this significant wave height evolution and therefore have accounted for the mean significant wave height decay along the propagation. This was observed to be 4.5cm for the largest propagation distance of 150km considered in this study and is consistent with previously studies of energy decay along the propagation by the use of the same instrument (Ardhuin et al. 2009). In the resulting dataset, we have verified that no bias dependent on propagation distance remains.

## 4.2 Buoy directional spectra estimation and partitioning

The buoy spectra are reconstructed from the heave spectra and the 4 first directional distribution moments using the Maximum Entropy Method (MEM) from Lygre and Krogstad, rather than the simple harmonic decomposition suggested in the NDBC documentation.

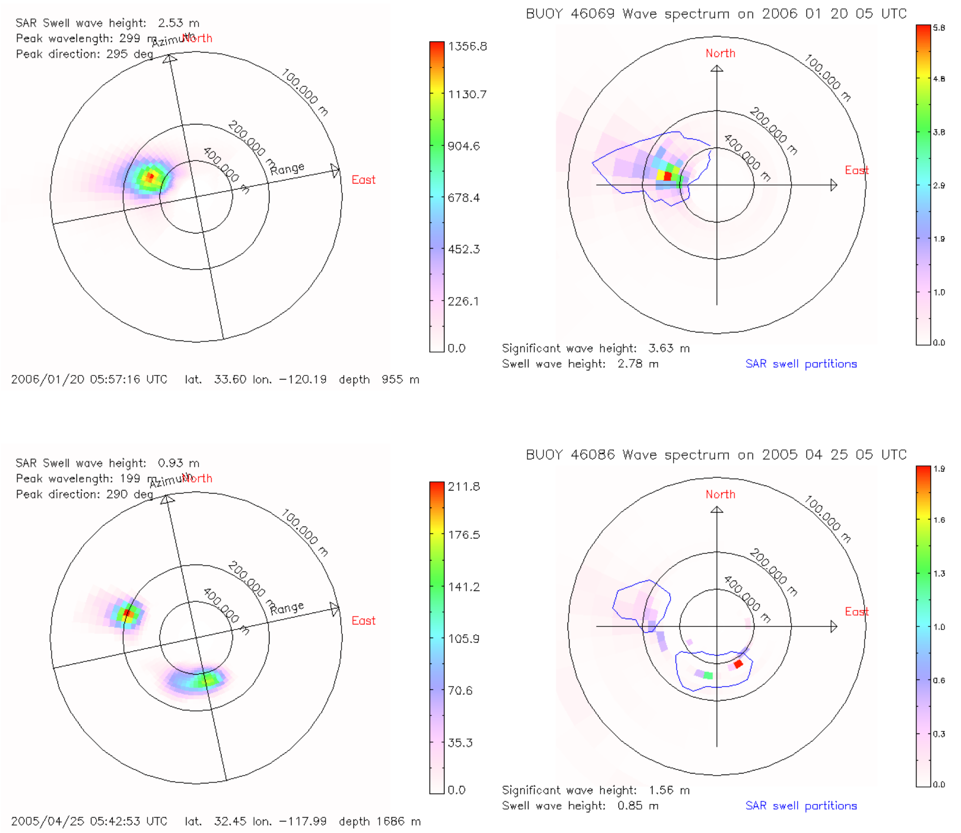


**Figure 4-1: (Left) Examples of SAR-derived swell spectra. (Right): Comparisons with collocated directional spectra extracted from buoy measurements. The blue contour, obtained after partitioning the SAR–derived wave spectrum, acts as a mask on which the comparison is done to be consistent.**

Each SAR spectrum (left) is partitioned using the usual inverted water-catchment procedure [Gerling, 1992] but with pre-processing according to Portilla 2009 to reduce the effect of noise and subsequently only the swell part is considered.

Each swell partition is considered in the buoy spectra (inside the blue contour on the buoy spectral plot (right). All integrated parameters are estimated from the spectral area inside the blue contour to ensure a comparison over corresponding swell systems.

For each wave spectrum observed in the world ocean, swell partitions are extracted providing estimations of Hss, Tp, and $\theta$p. In practice, the L2 spectra are first smoothed over 3 direction bins (30° sectors) and 3 wavenumber bins, in order to remove multiple peaks that actually correspond to the same swell system. The swell peak period is defined as the energy-weighted average around +-22% of the frequency with the maximum energy.

Likewise the peak direction $\theta p$ is defined as the energy weighted direction within 30◦ of the peak direction

## 4.3 Analysis method

Most of directional buoys are unfortunately located at relatively short distances from the coast (less than 100km) with shallow water within the co-location criteria distance. We therefore had to perform additional selection of angular sectors of each coastal buoy to identify the directions from which the swell system can reach the area around the buoy without being affected by shallow waters.

For a global validation, a direct comparison of swell parameters at a global scale (estimated from level 2 wave mode products) with buoy measurements at nearly the same place and time [Holt et al., 1998; Johnsen and Collard, 2004] has been done. Previous validations were presented for the total wave height Hs [Collard et al., 2005] or a truncated wave height $Hs_{12}$ defined by chopping the spectrum at a fixed frequency cut-off of 1/12 Hz. For that parameter, Johnsen and Collard [2004] found a root mean square (RMS) difference of 0.5 m, when comparing SAR against buoy data, including a bias of 0.2 m. In the present study, we use Hss values obtained from both SAR and buoy spectra.

A preliminary validation of Hss was performed by Collard et al. [2006], using L2 processing applied to 4 by 4 km tiles from narrow swath images exactly located at buoy positions.

That study found a 0.37 m rms error. This smaller error was obtained in spite of a 4 times smaller image area that should, on the contrary, produce larger errors due to statistical uncertainties. This suggests that a significant part of the ”errors” in SAR validation studies are due to the distance between SAR and buoy observations.

The swell height validation has been repeated in [Collard & Al 2009] using some buoy data from mostly NDBC sources between 2004 to 2008, located within 200 km and 1 hour of the SAR observation. These co-located data are made publically available as part of the XCOL project on the CERSAT ftp server, managed by Ifremer. Because they wished to avoid differences due to coastal sheltering and shallow water effects, they restricted their choice of buoys to distances from the coast and the 100 m depth contour larger than 100 km. As a result, most selected buoys were not directional, and partitions were derived in frequency only. Swell partition were therefore defined as the region between two minima of the frequency spectrum. The corresponding energy Es provided the swell height $Hss = 4\sqrt{Es}$. The buoy swell height was then defined from the energy contained within the frequency band of the SAR partition. The peak period was then estimated as the period where the buoy spectrum was maximal. The database included 15628 swell partitions observed by the SAR, with matched buoy swell partitions.

In the present study, thanks to the larger time span and the new technique of observation propagation, we can obtain a sufficient database of directional buoy measurements within a distance of 100km of the SAR observation or propagated observation.

Many of these observations correspond to relatively short swells, for which the waves are poorly imaged. We have thus defined a subset of the database by imposing the following 3 conditions:

- First the image normalized variance, linked to the contrast intensity and homogeneity, should be in the range 1.05 to 1.5. This removes SAR data with non-wave features (slicks, ships ...) that would otherwise contaminate the wave spectra.
- Second, both the SAR and buoy peak periods are restricted to the 12 to 18 s range, which removes most of the problems related to the azimuth cut-off.
- Third and last, the SAR derived wind speed U10SAR is limited to the range 3 to 9 $ms^{-1}$ in order to remove low winds with poorly contrasted SAR images, and high winds which may still cause some important azimuth cut-off and contamination of swell spectra by wind sea spectra.

A crucial difference with previous studies is that the bias on Hss was previously found to be primarily a function of the swell height and wind speed, increasing with height and decreasing with wind speed. In the present study a more detailed analysis has been performed and it was noticed that the bias function of wave height was also a function of dominant wavelength. Variations in standard deviation are dominated by the swell height and peak period, with the most accurate estimations for intermediate periods of 14 to 17 s.

## 4.4 Results

The wave parameters results are presented by buoy network. For each buoy network there are four plots as follows:

- Position of matchup data used with indication of distance from buoy.
- Results of SAR L2P calibrated significant wave height versus buoy
- Results of SAR L2P calibrated Dominant wavelength versus buoy
- Results of SAR L2P calibrated Dominant direction versus buoy

The sigma0/wind bias and RMS error are also estimated as function of wind speed.

### 4.4.1 NODC directional buoy network

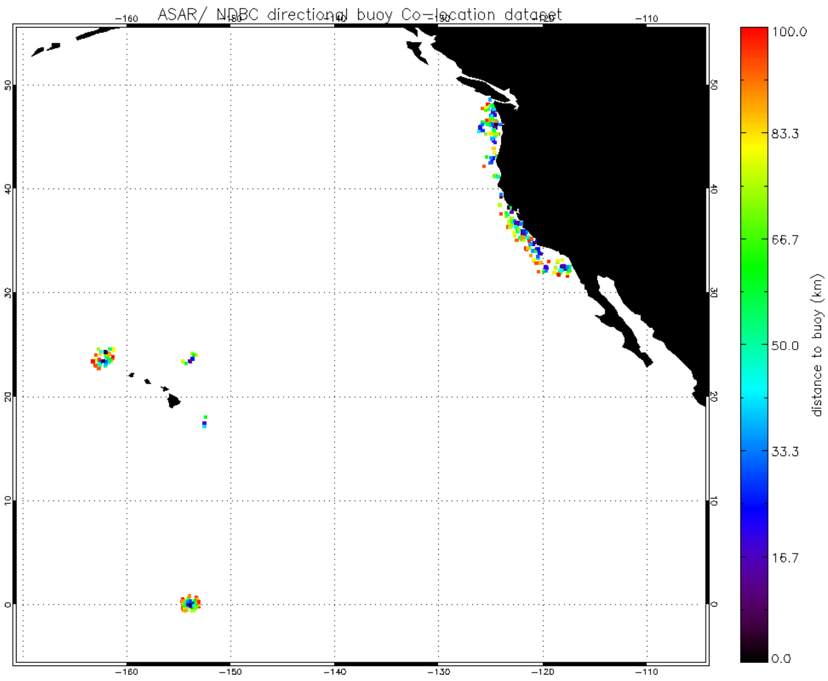


**Figure 4-2: Matchups for ENVISAT ASAR / NODC analysis**

Careful analysis of significant wave height bias using the GlobWave ASAR/NODC matchup database have highlighted a dependence of the calibration factor on dominant wavelength. The shorter wavelength has a larger Hss dependant bias than the longer one. The additional bias function of wind speed is found to be less than observed in previous studies. But it might be because that part of the wavelength dependant bias was considered to be dependent upon wind speed, since wind speed and dominant wavelength are not completely de-correlated.

calibrated Hss =

SAR_hss*(0.215+SAR_dwl/670.) +0.05*max(0,Wind_speed_SAR-7)-0.05

where SAR_dwl is the dominant observed wavelength for the considered swell partition

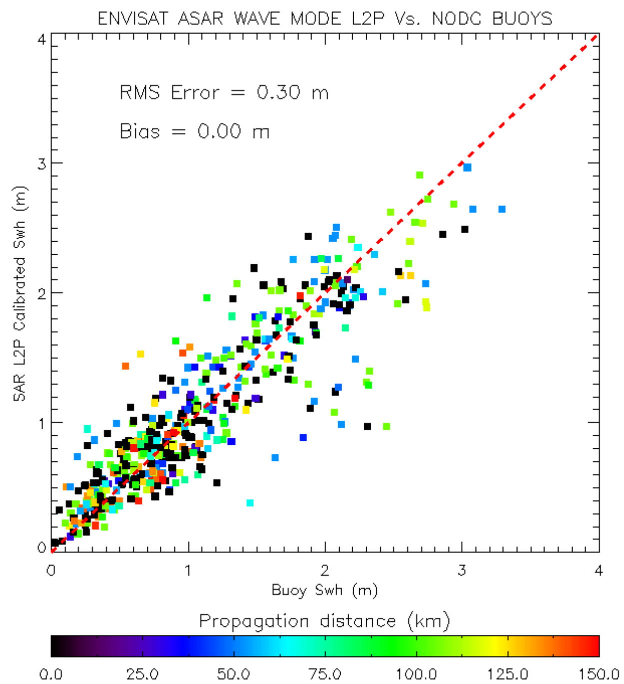


**Figure 4-3: Swell Significant wave height Hss from ENVISAT ASAR / NODC directional buoys matchups**

calibrated SAR_dwl = SAR_dwl*1.14-61

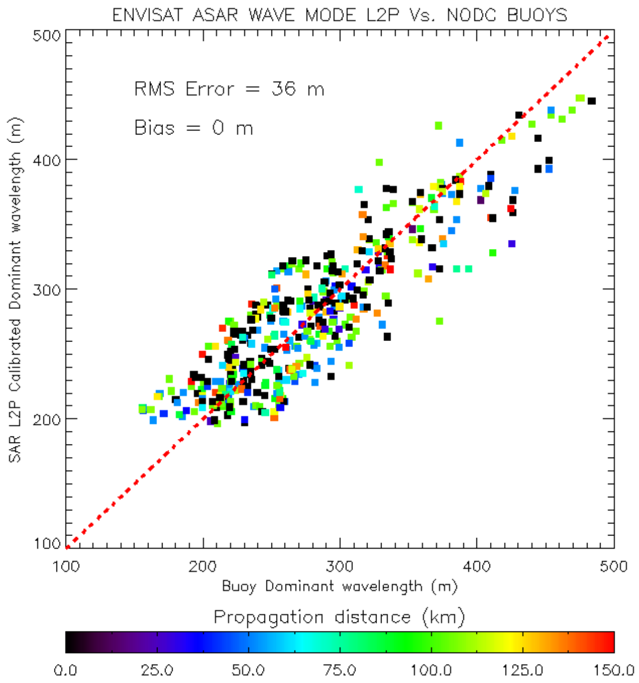

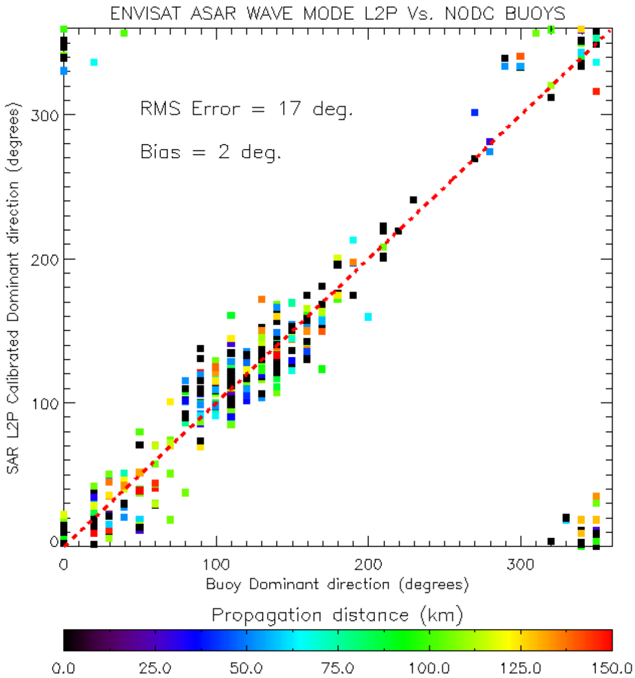


**Figure 4-4: Dominant direction from ENVISAT ASAR / NODC directional buoys matchups**

### 4.4.2 CDIP directional buoy network

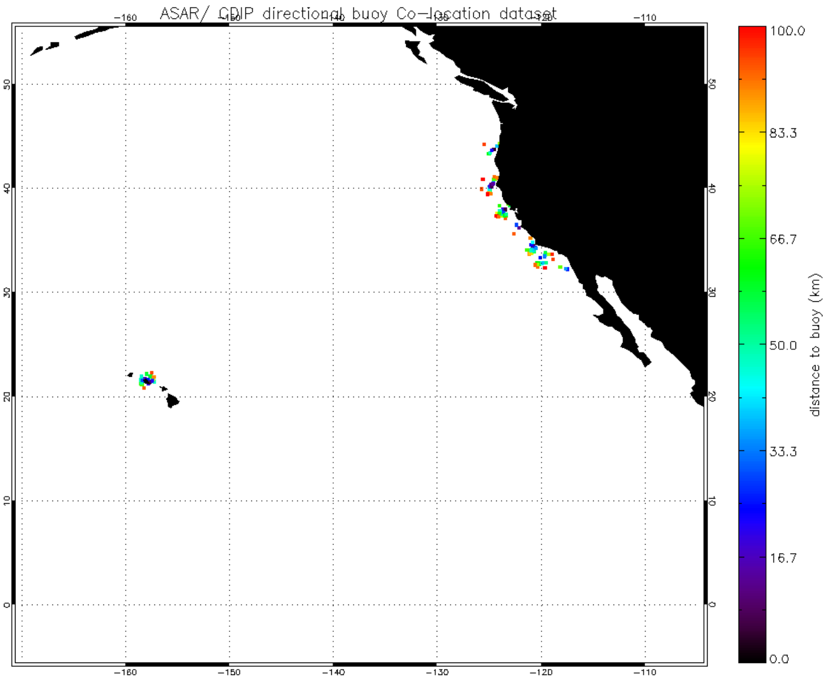


**Figure 4-5: Matchups for ENVISAT ASAR / CDIP analysis**

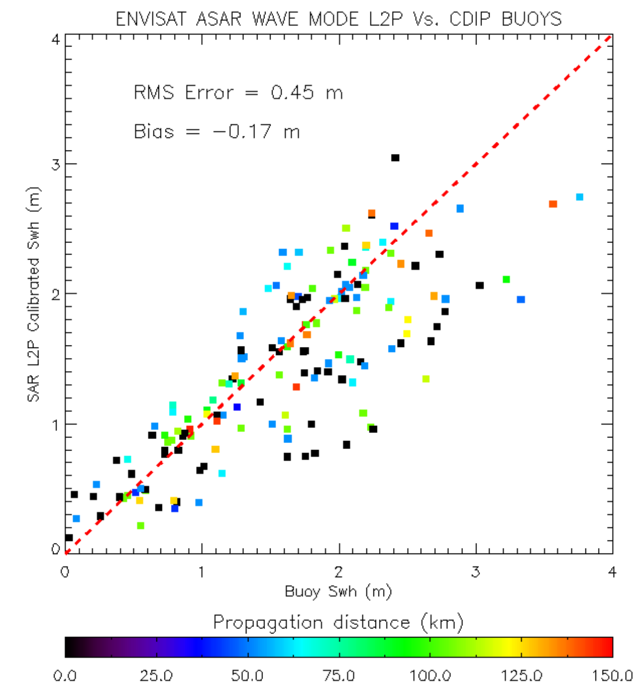


**Figure 4-6: Swell Significant wave height Hss from ENVISAT ASAR / CDIP directional buoys matchups**

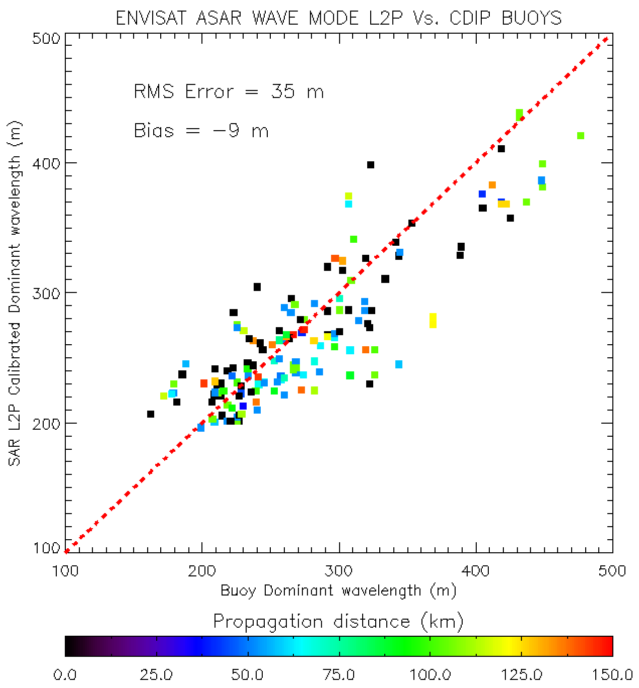


**Figure 4-7: Dominant wavelength from ENVISAT ASAR / CDIP directional buoys matchups**

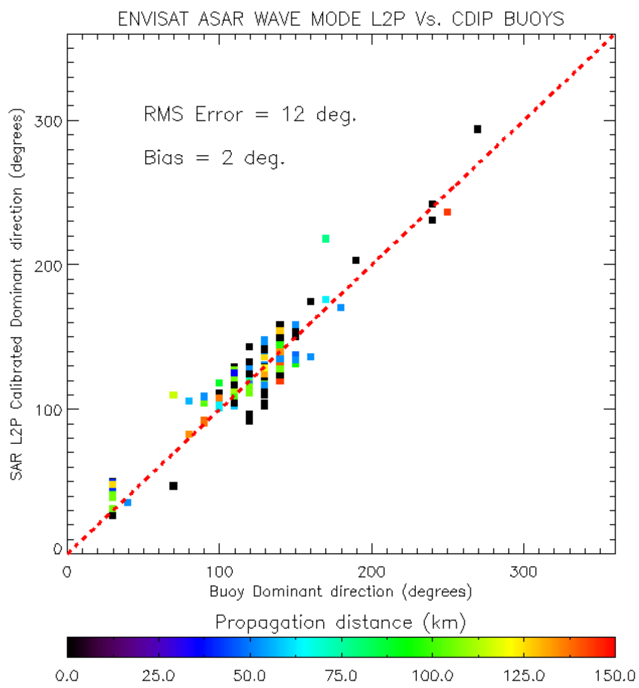


**Figure 4-8: Dominant direction from ENVISAT ASAR / CDIP directional buoys matchups**

### 4.4.3 Significant wave height, dominant wavelength and direction error characterisation results

Careful analysis of significant wave height bias using the ASAR/NODC and ASAR/CDIP matchup databases have highlighted a dependence of the calibration factor on dominant wavelength. The shorter wavelength has a larger Hss dependant bias than the longer one. The additional bias function of wind speed is found to be less than observed in previous studies. But it might be that part of the wavelength dependant bias was considered to be dependent upon wind speed since wind speed and dominant wavelength are not completely de-correlated.

calibrated Hss =

SAR_hss*(0.215+SAR_dwl/670.) +0.05*max(0,Wind_speed_SAR-7)-0.05

where SAR_dwl is the dominant observed wavelength for the considered swell partition

calibrated SAR_dwl = SAR_dwl*1.14-61

The bias of the mean direction (2deg) is not significant compared to the accuracy of the measurement where the direction is provided on a 10 deg grid bin.

There was not sufficient collocated data to really assess the change of RMS error by bins of values so the RMS error is considered as the following:

Hss RMS error = 0.30m

Dominant wavelength RMS error = 37m

Dominant Direction RMS error = 17 deg

### 4.4.4 Sigma0 and wind speed error characterisation results

Calibration and error characterisation of sigma0 and wind speed is based on the CMOD IFREMER Geophysical model that relates wind speed, wind direction, incidence angle and Normalized Radar Cross Section. From an independent source of wind vector information (here ECMWF analysis) and under a particular geometrical configuration, one can compute the expected Cross section and compare it with the observation in L2P products.

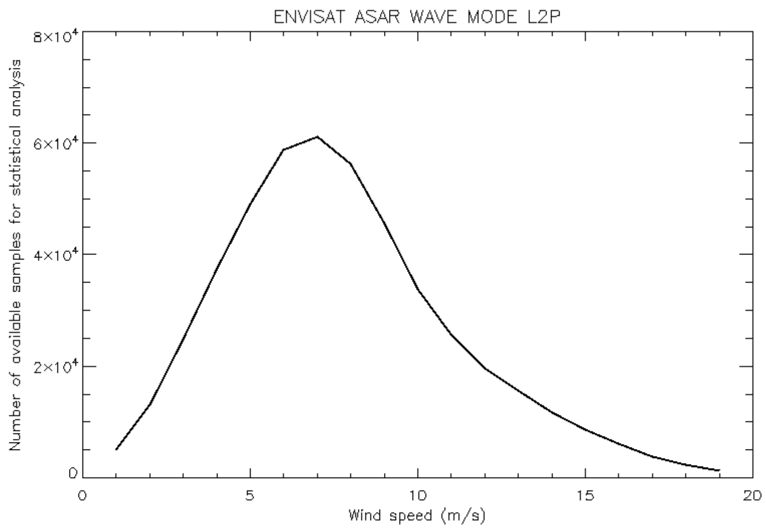


**Figure 4-9: Distribution of wind speed in the SAR L2P dataset**

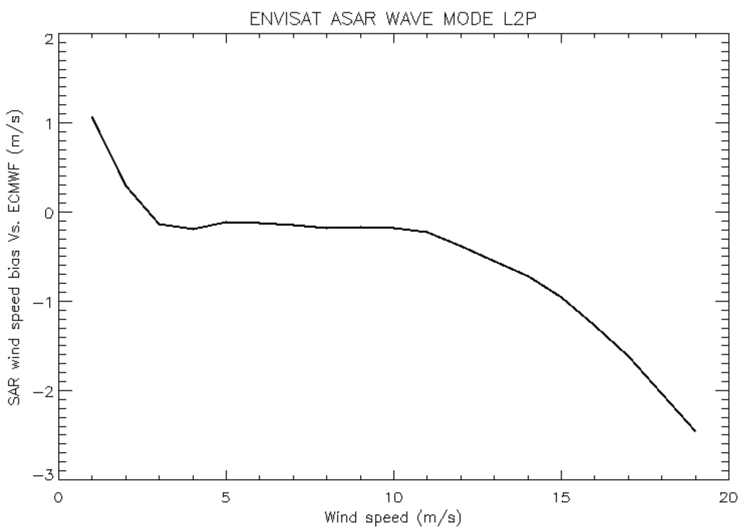


**Figure 4-10: Evolution of SAR wind speed bias of as function of wind speed**

No significant wind speed bias (-0.2m/s) is observed for wind speeds ranging from 3 to 11m/s but a rather large overestimation and underestimation is seen at low and high wind speeds respectively.

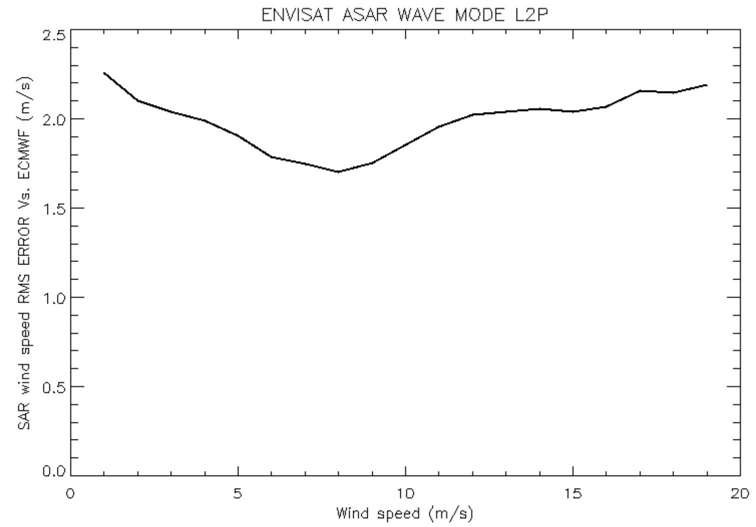


**Figure 4-11: Evolution of SAR wind speed RMS error of as function of wind speed**

The overall usual 2m/s RMS error for SAR wind speed is observed. A slightly better comparison is observed around 7m/s corresponding to the most commonly encountered wind speed.

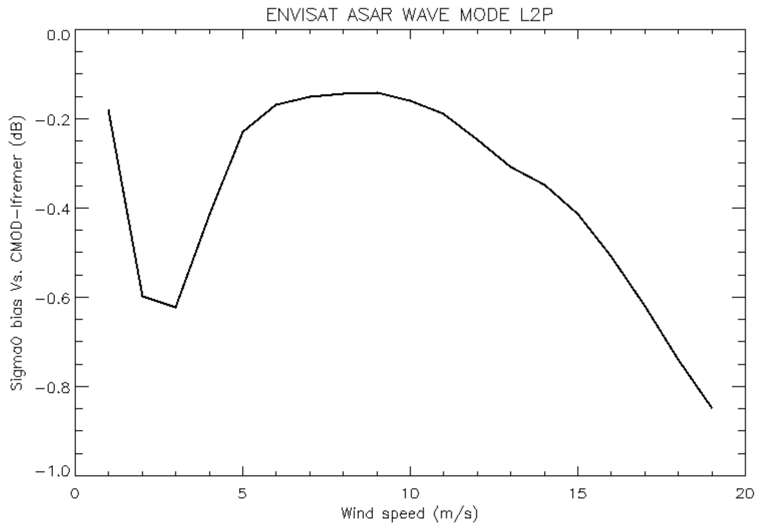


**Figure 4-12: Evolution of SAR sigma0 RMS error of as function of wind speed**

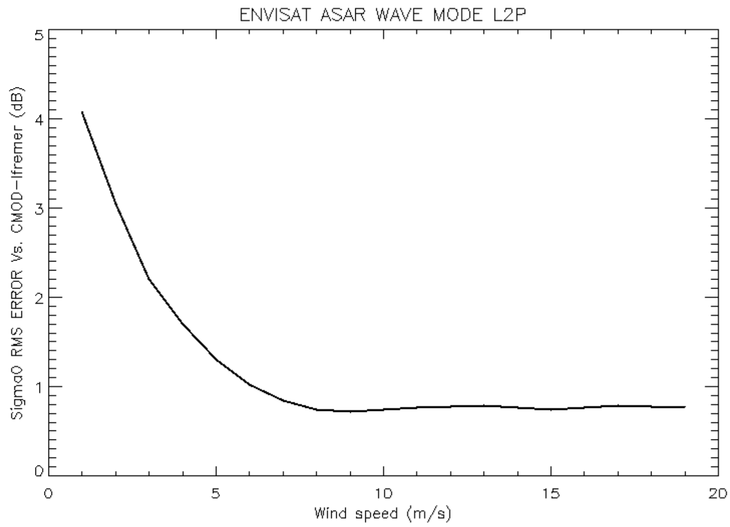


**Figure 4-13: Evolution of SAR sigma0 RMS error of as function of wind speed**

The relatively large RMS error on the mean sigma0 estimated over SAR imagettes at low wind speed is caused by the large sensitivity of the first generated surface waves at low wind to the presence of surfactant on the sea surface. For a given low wind of 2m/s, under certain conditions when higher winds has just stopped, there is very little chance of surfactant and the backscatter coefficient will be quite high whereas if the water was calm since a long time, surfactant may cover the surface damping the short waves and sometimes reducing the NRCS down to the noise floor.

## 4.5 References

Collard, F., B. Chapron, F. Ardhuin, H. Johnsen, and G. Engen (2006), Coastal ocean wave retrieval from ASAR complex images, in Proceedings of OceanSAR, Earth Observation Marine Surveillance Coordination Comittee, Saint John's, Canada.

Collard, F., F. Ardhuin, and B. Chapron (2009), Monitoring and analysis of ocean swell fields from space: New methods for routine observations, *J. Geophys. Res.,* 114, C07023, doi:10.1029/2008JC005215.

Gerling, T.W.: Partitioning sequences and arrays of directional wave spectra into component wave systems, J. Atmos. Oceanic Technol., 1992, 9: 444-558.

Holt, B., A. K. Liu, D. W. Wang, A. Gnanadesikan, and H. S. Chen (1998), Tracking storm-generated waves in the northeast pacific ocean with ERS-1 synthetic aperture radar imagery and buoys, J. Geophys. Res., 103(C4), 7917–7929.

Johnsen, H., and F. Collard (2004), ASAR wave mode processing - validation of reprocessing upgrade. technical report for ESA-ESRIN under contract 17376/03/I-OL, Tech. Rep. 168, NORUT.

LYGRE, A. and KROGSTAD, H.E. (1986). Maximum entropy estimation of the directional distribution in ocean wave spectra, J. Phys. Ocean., 16, 2052-2060.

Jesús Portilla, Francisco J. Ocampo-Torres, Jaak Monbaliu. (2009) Spectral Partitioning and Identification of Wind Sea and Swell. Journal of Atmospheric and Oceanic Technology 26:1, 107-122.

# 5 SATELLITE CROSSOVER ANALYSIS

This section gives presents the delayed-mode L2P intercomparison based on the analysis of altimeter crossover data.

## 5.1 Satellite crossover data

Satellite crossover data has been computed at Ifremer for altimetry data according to the following satellite combinations.

| | GFO | ERS-1 | ERS-2 | TOPEX / Poseidon | Jason-1 | Jason-2 | Envisat |
|---|---|---|---|---|---|---|---|
| GFO | | | | | | | |
| ERS-1 | | | | | | | |
| ERS-2 | | | | | | | |
| TOPEX / Poseidon | | | | | | | |
| Jason-1 | | | | | | | |
| Jason-2 | | | | | | | |
| Envisat | | | | | | | |

**Table 5-1: Availability of altimeter crossover data**

The key for the satellite combinations is as follows:

- Orange - no match-ups produced because the mission time frames do not overlap
- Yellow - no match-ups because the satellites share a common track
- Green - match-ups are available

There are no SAR crossovers since the ERS-2 SAR and ENVISAT ASAR instruments share a common orbit track.

The collocation criteria are maximum distance of 60km and maximum time difference of 1 hour. This criteria is the result of a trade-off between having the best spatial and temporal proximity between each sensor’s measurements and having a sufficient number of match-ups to provide statistically relevant estimates of errors. However very few distances were > 5km, so the analysis described below were restricted to those data with collocation distances < 5km.

Data include both nearest values and additional along-track data points either side, and the spatial and temporal differences between the match-ups are stored along with their values.

## 5.2 Analysis method

Analysis was carried out on altimetry significant wave height values. For most crossover combinations a representative sample of data has been analysed.

Typically this is a one-year period containing a few thousand samples. Where an altimeter is known to have changed its calibration or sensor side during the mission, such as with TOPEX, additional years have been analysed. For Jason-1 combinations with ERS-2, Envisat and GFO all years were analysed. A representative year is presented here and any major variations between years discussed in the text.

Data pairs are plotted and Orthogonal Distance Regression performed in order to quantify differences between the sensor measurements. Calibrated Hs values (from the swh_calibrated variable in the L2P data) are used in order to identify any issues with the GlobWave calibrations.

# 5.3 Results

## 5.3.1 ERS-1 combinations

For ERS-1 there are just crossovers with TOPEX/Poseidon. The results are shown in Figure 5-1.

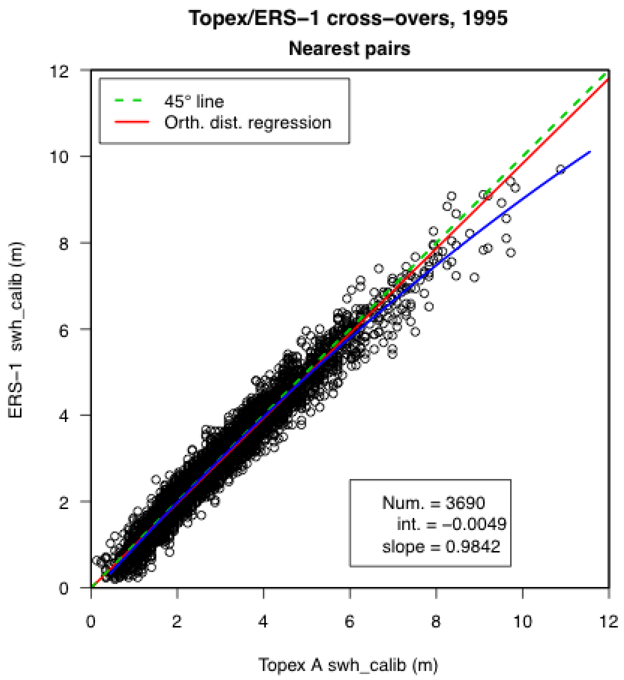


**Figure 5-1: ODR analysis of TOPEX/ERS-1 crossover pairs from 1995**

The calibration agreement is good for significant wave heights below 6m, differing by less than 2%, however there is a non-linearity for values above 6m and here a quadratic fit is more appropriate (see blue line). This observation warrants further investigation.

## 5.3.2 ERS-2 combinations

For ERS-2 there are crossovers with TOPEX/Poseidon, GFO, Jason-1 and Jason-2.

With the TOPEX altimeter there were changes in the calibration over time due to sensor drift then a change of sensor side. Because of this the TOPEX/ERS-2 analysis is performed for three different years.

ERS-2 combinations with TOPEX, GFO and Jason-2 demonstrate good agreement, slopes are within 1.5% and offsets within 7cm.

With Jason-1 there are slightly larger differences, 2.4% slope and 14cm offset. This is representative of the complete analysis from 2002 to 2009 and there is little variation between years.

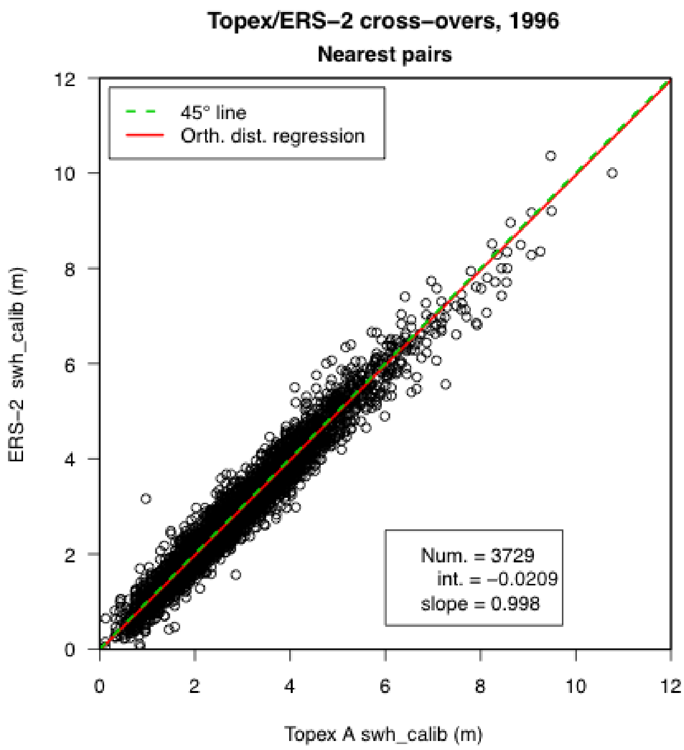


**Figure 5-2: ODR analysis of TOPEX/ERS-2 crossover pairs from 1996**

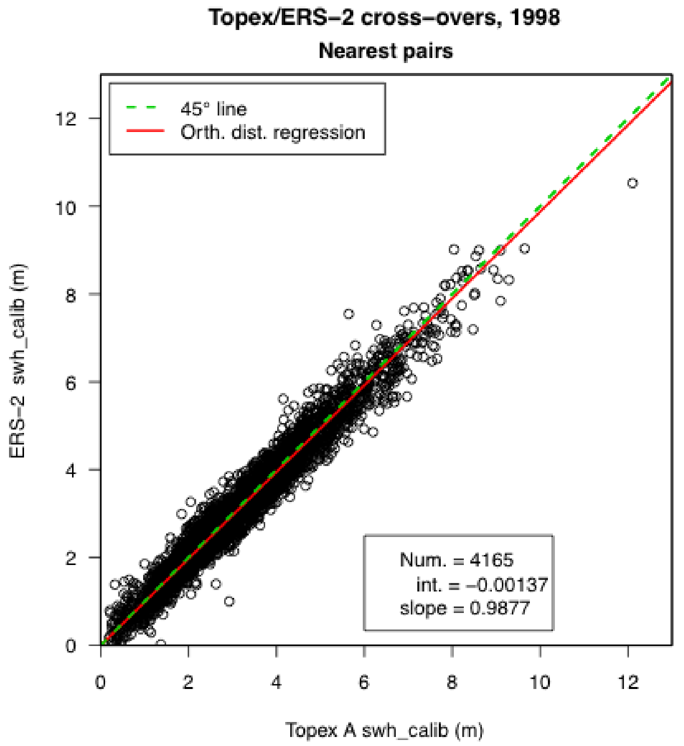


**Figure 5-3: ODR analysis of TOPEX/ERS-2 crossover pairs from 1998**

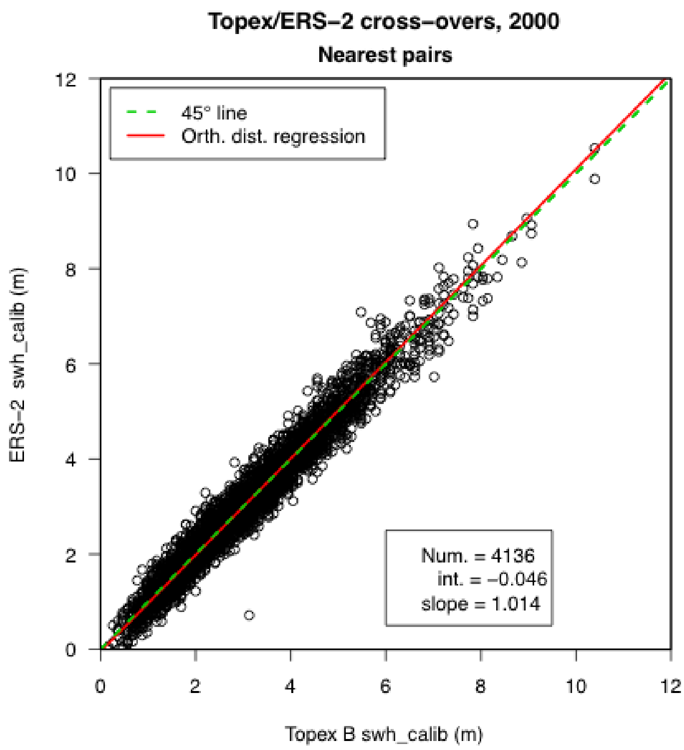


**Figure 5-4: ODR analysis of TOPEX/ERS-2 crossover pairs from 2000**

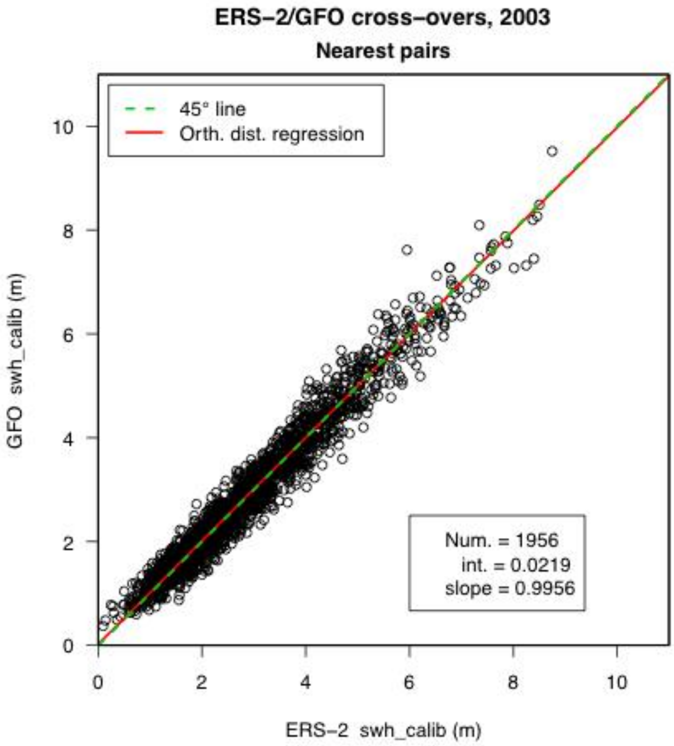


**Figure 5-5: ODR analysis of ERS-2/GFO crossover pairs from 2003**

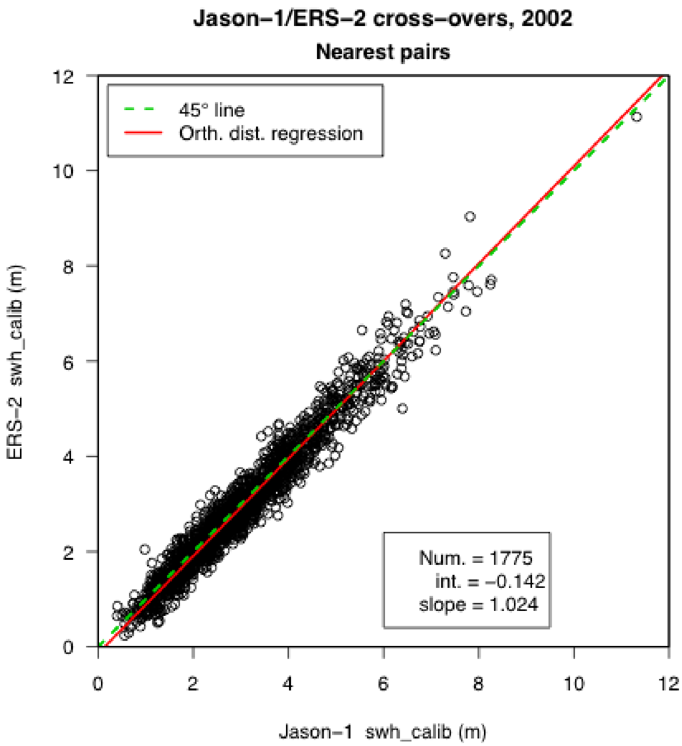


**Figure 5-6: ODR analysis of ERS-2/Jason-1 crossover pairs from 2002**

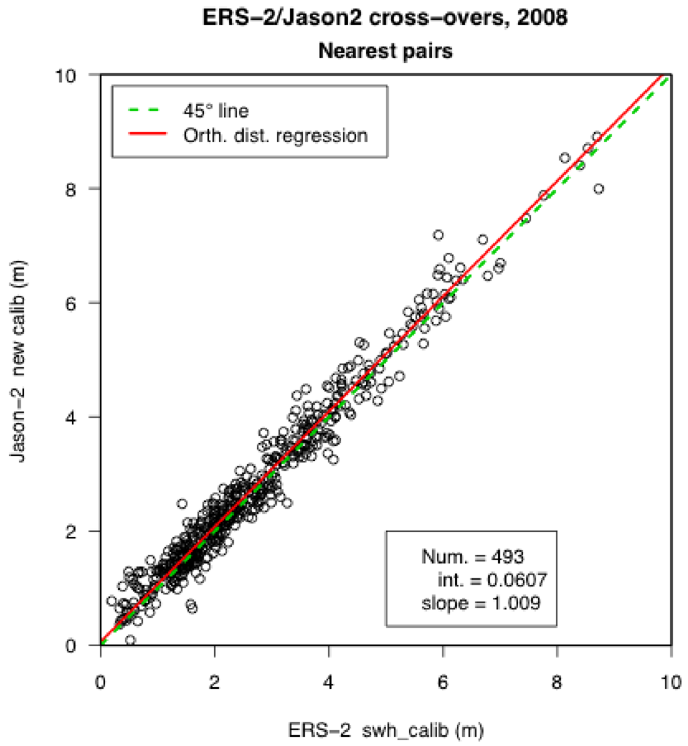


**Figure 5-7: ODR analysis of ERS-2/Jason-2 crossover pairs from 2008**

### 5.3.3 Envisat combinations

For Envisat there are crossovers with TOPEX/Poseidon, GFO, Jason-1 and Jason-2.

In all cases slopes are within 1.5% and offsets within 11cm. The agreement between Envisat and GFO is especially good.

The comparison with Jason-1 was conducted for all years (2003 to 2009) and the example shown from 2007 is representative of the complete analysis. A summary of the results for each year is given in Table 5-2. There is little variation between years.

The final Envisat plot (Figure 5-12) shows a comparison with Jason-2 when both altimeters are calibrated according to the new calibrations obtained from the errors analysis in the previous section. In this case there is hardly a difference between the regression and 45 degree line.

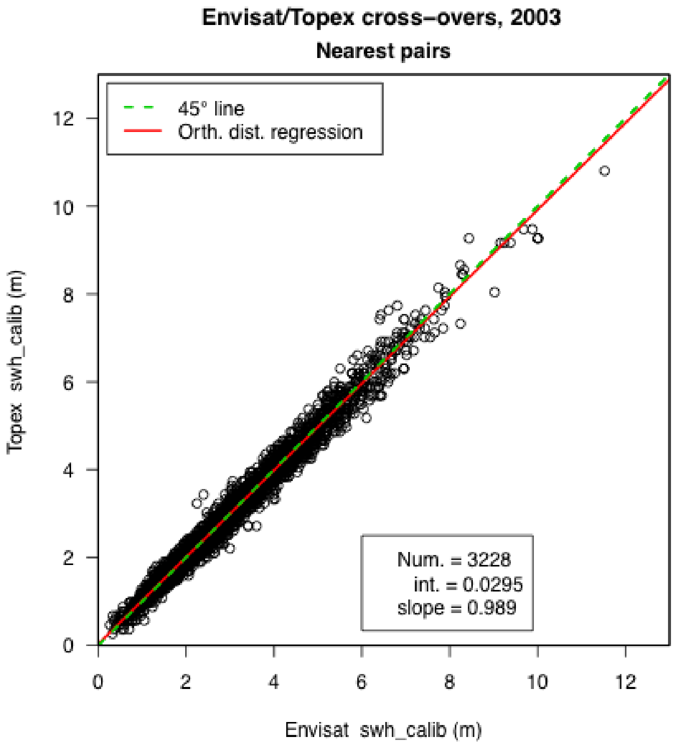


**Figure 5-8: ODR analysis of Envisat/TOPEX crossover pairs from 2003**

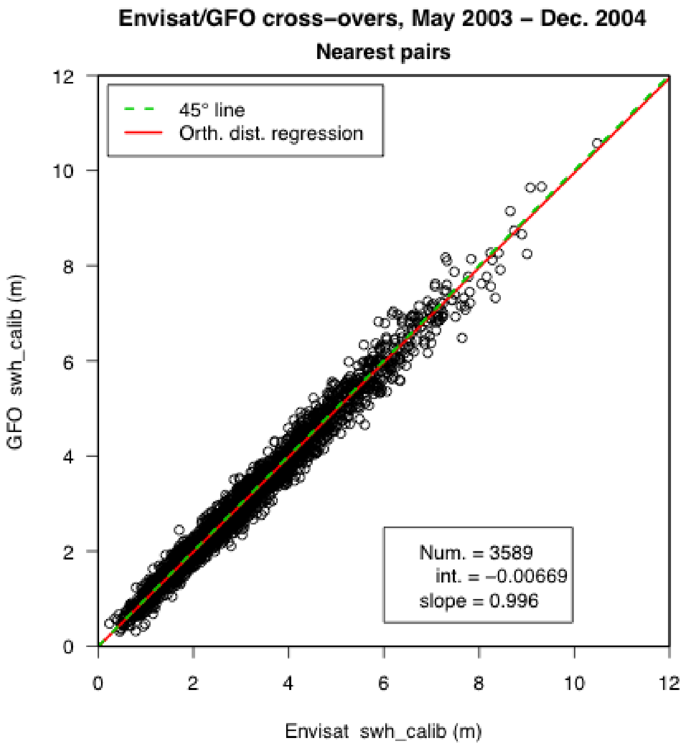


**Figure 5-9: ODR analysis of Envisat/GFO crossover pairs from 2003/2004**

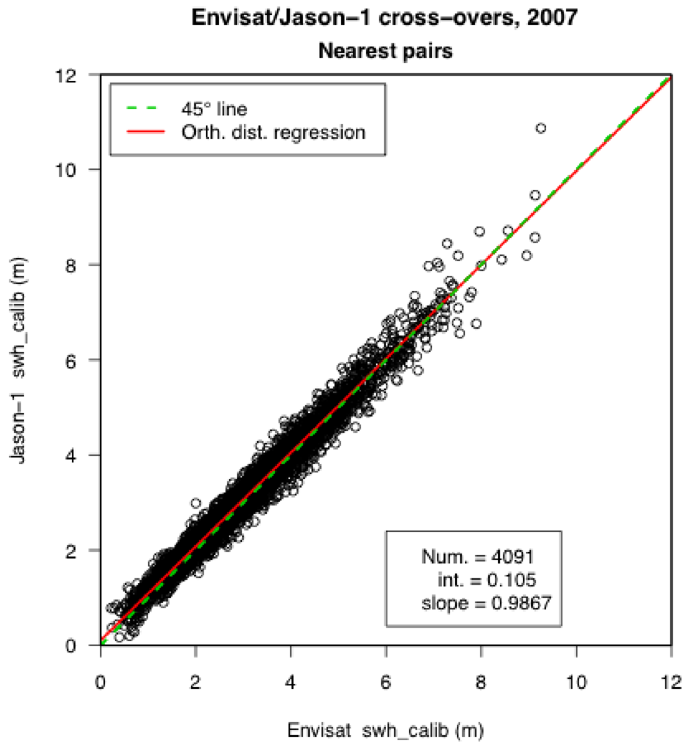


**Figure 5-10: ODR analysis of Envisat/Jason-1 crossover pairs from 2007**

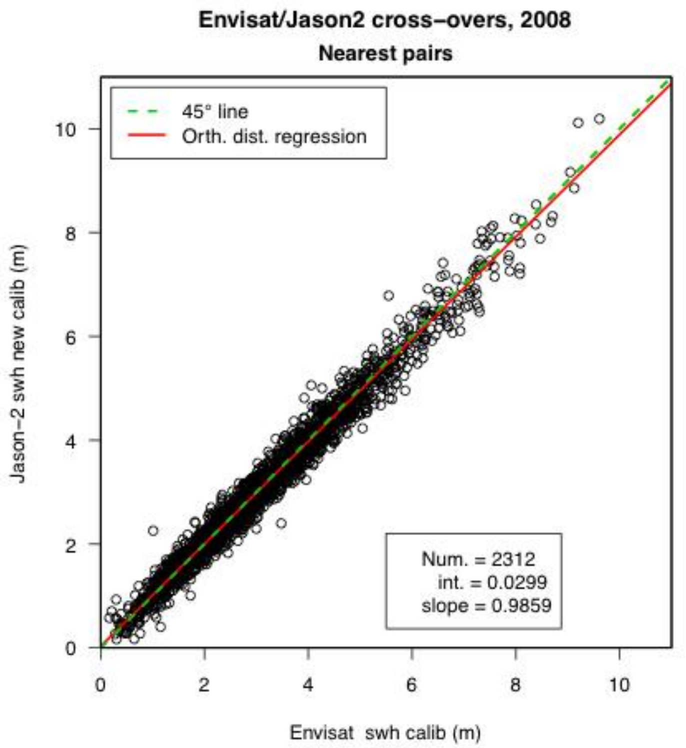


**Figure 5-11: ODR analysis of Envisat/Jason-2 crossover pairs from 2008**

| Year | Number data pairs | Regression formula |
|---|---|---|
| 2003-2009 | 24104 | 0.117 + Hs*0.987 |
| 2003 | 3299 | 0.147 + Hs*0.979 |
| 2004 | 3986 | 0.108 + Hs*0.990 |
| 2005 | 2524 | 0.088 + Hs*0.999 |
| 2006 | 3213 | 0.128 + Hs*0.981 |
| 2007 | 4091 | 0.105 + Hs*0.987 |
| 2008 | 4004 | 0.124 + Hs*0.985 |
| 2009 | 2987 | 0.110 + Hs*0.989 |

**Table 5-2: Summary of analysis of Envisat/Jason-1 crossover pairs by year**

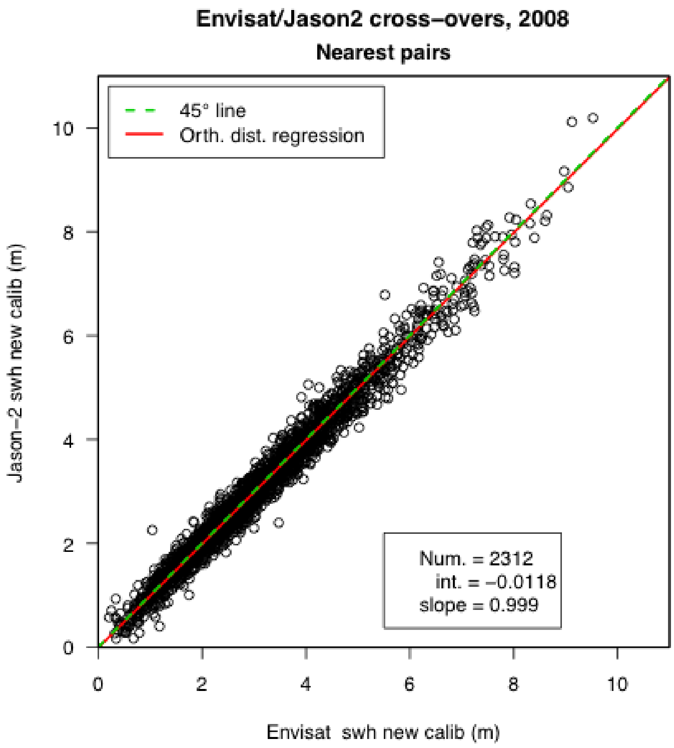


**Figure 5-12: ODR analysis of Envisat/Jason-2 crossovers with calibrations from GlobWave error analysis**

## 5.3.4 GFO combinations

For GFO there are additional crossovers with TOPEX/Poseidon and Jason-1.

The comparison with TOPEX/POSEIDON was conducted for all years (1998 to 2005) and the example shown from 2003 is representative of the complete analysis as there is little variation between years. The very good agreement is not surprising, since the GFO calibration coefficients were obtained by Queffeulou & Croizé-Fillon (2009) from a comparison of GFO wave heights with those from Topex and ERS-2.

For the GFO/Jason-1 comparison the differences for 2005 are similar to the ERS-2/Jason-1 combination with 2.3% slope and 13cm offset. This is representative of the analysis from 2002 to 2007 and there is little variation between these years. However the 2008 analysis showed much larger differences with over 14% of slope and 43cm offset. GFO had control problems towards the end of the mission; and this analysis suggests that Hs data from 2008 should be discarded. A summary of the results for each year is given in Table 5-3.

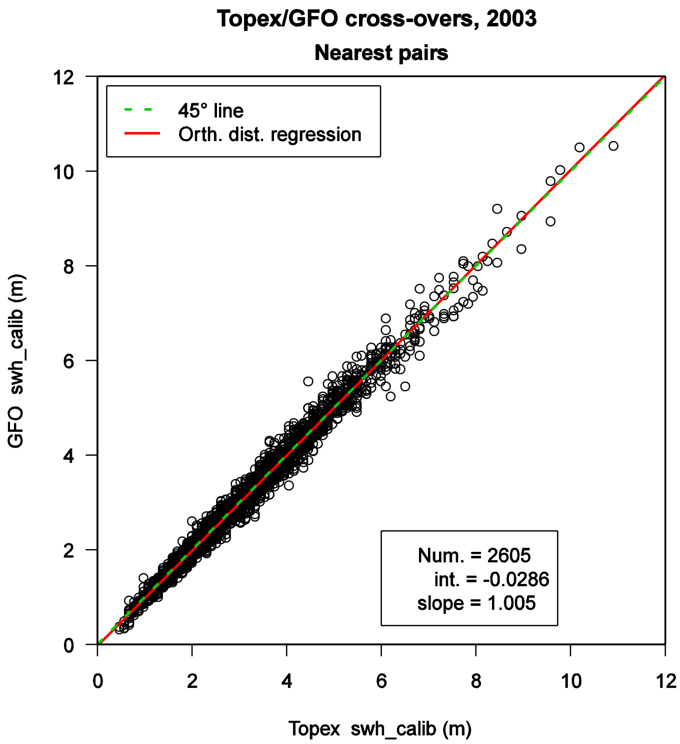


**Figure 5-13: ODR analysis of GFO/TOPEX crossover pairs from 2003**

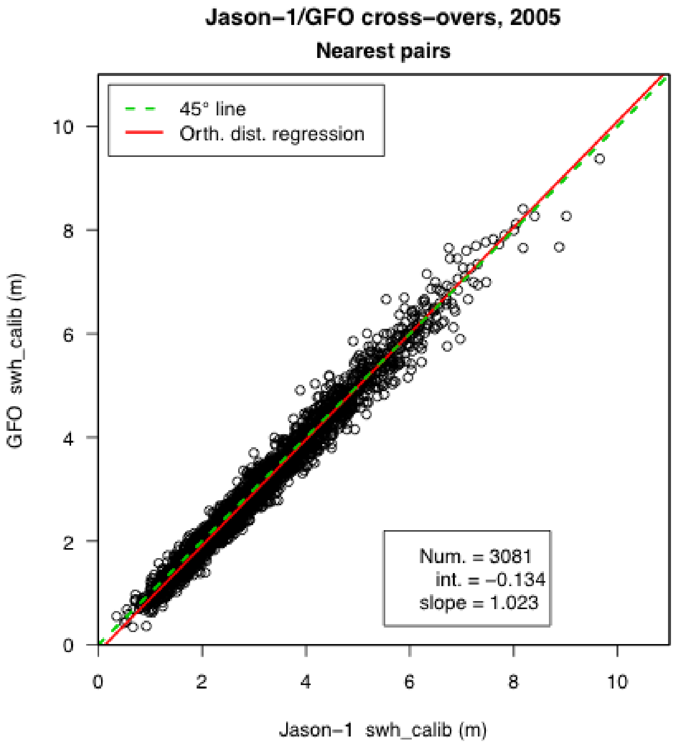


**Figure 5-14: ODR analysis of GFO/Jason-1 crossover pairs from 2005**

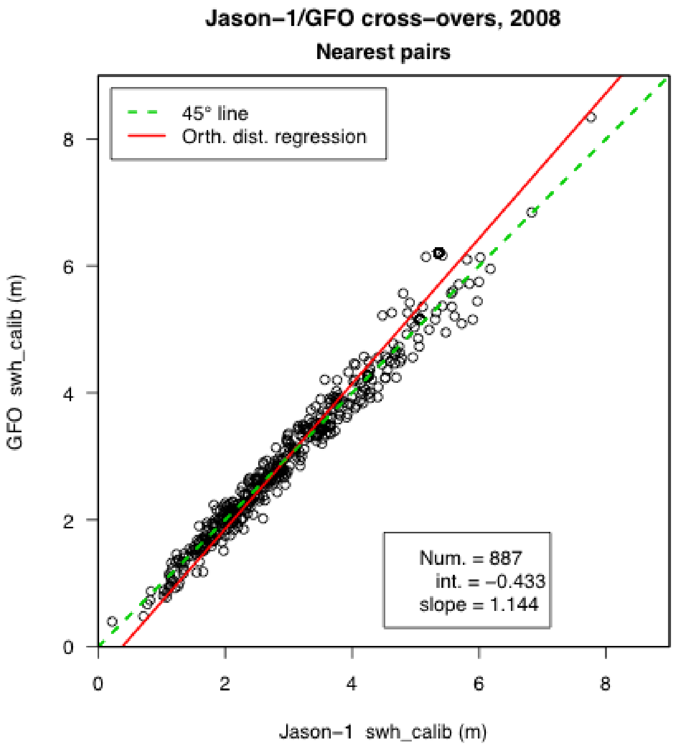


**Figure 5-15: ODR analysis of GFO/Jason-1 crossover pairs from 2008**

| Year | Number data pairs | Regression formula |
|---|---|---|
| 2003-2007 | 12836 | -0.126 + Hs*1.021 |
| 2002 | 1505 | -0.145 + Hs*1.026 |
| 2003 | 2808 | -0.138 + Hs*1.023 |
| 2004 | 2672 | -0.122 + Hs*1.018 |
| 2005 | 3081 | -0.134 + Hs*1.023 |
| 2006 | 2666 | -0.118 + Hs*1.019 |
| 2007 | 1609 | -0.110 + Hs*1.025 |
| 2008 | 887 | -0.443 + Hs*1.144 |

**Table 5-3: Summary of analysis of GFO/Jason-1 crossover pairs by year**

**Company Address**

Logica UK Ltd.
Keats House
The Office Park
Springfield Drive
Leatherhead
Surrey
KT22 7LP

**Contact person:**

Dr. Geoff Busswell
GlobWave Project Manager

P: +44 (0) 7595 612 392
F: +44 (0) 1372 759 890

E: geoff.busswell@logica.com
www.logica.com